Received: 4 March 2022 | Revised: 25 May 2022 | Accepted: 18 June 2022

DOI: 10.1002/aoc.6799

RESEARCH ARTICLE

Applied Organometallic Chemistry WILEY

Physical–chemical studies of new, versatile carbazole derivatives and zinc complexes: Their synthesis, investigation of in vitro inhibitory effects on α-glucosidase and human erythrocyte carbonic anhydrase I and II isoenzymes

Sümeyye Çol[1] | Mustafa Emirik[2] | Zuhal Alım[3] | Arif Baran[1]

[1]Faculty of Arts and Sciences, Chemistry Department, Sakarya University, Sakarya, Turkey

[2]Faculty of Arts and Sciences, Chemistry Department, Recep Tayyip Erdoğan University, Rize, Turkey

[3]Faculty of Arts and Sciences, Chemistry Department, Ahi Evran University, Kırşehir, Turkey

Correspondence
Prof. Dr. Arif Baran, Sakarya University, Department of Chemistry, 54187, Sakarya, Turkey.
Email: abaran@sakarya.edu.tr.

Funding information
Scientific and Technological Research Council of Turkey, Grant/Award Numbers: KBAG-217Z043, KBAG-115Z446; TUBITAK, Grant/Award Number: BIDEB/2211-C; Sinop University Research Center; Sakarya University, Grant/Award Number: 2022-7-25-3

In this study, two novel zinc–phthalocyanine complexes (**4a** and **6a**), containing carbazole rings, were investigated. The first phthalocyanine **4a** has been synthesized from 4-(2-(3-acetyl-9H-carbazol-9-yl)ethoxy at the peripheral position. Likewise, the second phthalocyanine **6a** has been synthesized from 4-(2-(3-cinnamoyl-9H-carbazol-9-yl)ethoxy at the same position. The new phthalocyanines (Pcs) and their ligands are soluble in organic solvents, such as dimethylformamide, dimethyl sulfoxide, dichloromethane, ethyl acetate, and methanol/ethanol. The Zn (II) complexes were characterized by Fourier transform infrared spectroscopy, nuclear magnetic resonance (NMR) (except ^{13}C NMR for complexes), elemental analysis, mass spectrometry, and UV–Vis spectroscopy. Also, photophysical and photochemical properties and cyclic voltammogram for the *N*-substituted carbazole zinc–Pcs have been reported. The evaluation of carbazole Zn (II) complexes (**4a** and **6a**) and ligands (**3**, **4**, **5,** and **6**) for in vitro α-glucosidase inhibitory activities was performed compared to standard drugs acarbose, and kinetic studies were also carried out to determine their inhibition modes. The inhibitory effects of these new Pcs (**4a** and **6a**) and their ligands (**3**, **4**, **5,** and **6**) on human erythrocytes carbonic anhydrase I (hCA I) and II (hCA II) isoenzymes were investigated. Moreover, in silico studies were also carried out to better investigate the interactions of *N*-substituted carbazole containing zinc Pcs with the active sites of hCA I and II isoforms.

KEYWORDS
carbazole zinc phthalocyanine, carbonic anhydrase, molecular docking, photophysical and photochemical properties, α-glucosidase

1 | INTRODUCTION

Phthalocyanines (Pcs) are an important class of tetrapyrrole compounds that continue to attract attention in various scientific fields due to their photochemical properties resulting from their aromatic and strong 18-π electronic structure.[1–3] The core of Pcs comprises four nitrogen atoms, and its nucleus can coordinate almost all metal ions. This shows that its macrocycle has a wide range of features.[2] Additionally, Pcs, which are chemically and

thermally stable, have been used as agents in various technological applications, such as optical devices,[4] solar cells,[5] biosensors,[6] catalysts,[7] photovoltaics, liquid crystals,[8] and photosensitizers in photodynamic therapy (PDT).[9,10] Among these applications, PDT, which plays a central role in cancer treatment, has gained popularity.[11] PDT depends on parameters, such as high singlet oxygen yield, high absorption at red wavelength, solubility, and high selectivity toward cancerous tissues.[12] The substituents containing alkyl or alkoxy groups can be added to the peripheral and non-peripheral positions of phthalocyanine structures to increase the solubility.[13,14] Among the diamagnetic metals in the phthalocyanine core, the Zn (II) metal ion is of interest due to its photophysical, photochemical, and enzyme inhibition properties and high singlet oxygen producing in PDT.[15–17] Considering these properties of the Zn (II) metal complex, it aims to synthesize new photosensitizing zinc Pcs with a long wavelength absorption, high singlet oxygen yield, suitable fluorescent quantum yield, and photodegradation quantum yield for PDT. The absence of carbazole Zn (II) Pcs in the literature on enzyme inhibition studies has enabled us to focus on this subject.

Recent research on Pcs has focused on applications, such as antioxidant, anticancer, antifungal, and enzyme inhibition.[18,19] However, as far as we know, there are few studies that examine the enzyme inhibitory effect and anticancer activities of carbazole-substituted phthalocyanine compounds. Barut et al. found that some peripheral or non-peripheral tetra-[4-(9H-carbazol-9-yl) phenoxy]-substituted cobalt (II), and manganese (III) phthalocyanine derivatives indicated activity against acetylcholinesterase, butyrylcholinesterase, α-glucosidase, and anticancer.[20] Goksel et al. examined novel zinc (II) Pcs and their quaternized derivatives that are bound by four or eight carbazole ring systems against hepatocarcinoma (HuH–7) cancer cell lines.[21]

Since carbazole and its derivatives contain electroactive nitrogen atoms, they constitute an essential class of aromatic heterocyclic compounds with photoconductivity and luminescence properties. Additionally, they are widely used in various industries, such as photoactive and electroactive materials, solar cells, electrochemistry, and polymers. Moreover, they are well-known in medicinal chemistry for their pharmacological activity properties, such as antipsychotic, antitumor, antioxidant, antibacterial, antidiabetic, anticonvulsant, and anti-inflammatory effects.[22–26] Some synthetic and natural carbazole derivatives are potent α-glucosidase inhibitors.[27]

Several studies found that carbazole-derived compounds showed inhibitory effects on α-glucosidase and carbonic anhydrase isoenzymes (CA I and CA II).[28,29] Although inhibition properties of carbazole-substituted Pcs on the α-glucosidase enzyme were reported, these properties in the carbonic anhydrase enzyme were not reported in the literature. Therefore, this study focused on investigating both α-glucosidase and carbonic anhydrase inhibition properties with novel carbazole-substituted Zn–Pcs. In recent studies on the α-glucosidase and carbonic anhydrase isoforms inhibition of non-sugar, easily synthesized molecules have attracted attention.[30a]

Diabetes mellitus (DM) is a chronic endocrine disorder that disrupts carbohydrate, protein, and fat metabolism. It is indicated by hyperglycemia, which can be detected by high blood sugar levels.[30b] α-Glucosidase is one of the enzymes that is used to treat Type II DM and is involved in carbohydrate metabolism. This enzyme reduces postprandial hyperglycemia (PPHG) by inhibiting the carbohydrase enzymes of PPHG.[30c] The α-glucosidase enzyme has proven to be a promising therapeutic target for diabetes, which is currently one of the most common health problems that affect millions of people worldwide, especially in the developing countries. For the treatment of these diabetic diseases, voglibose, miglitol, and acarbose, which are known as sugar ring-based α-glucosidase inhibitors, are used.[31–33,34a] Initially, α-glucosidase enzyme inhibition studies were performed by synthesizing sugar imitation molecules, and the results were corrected by performing an enzyme kinetic study. α-Glucosidase inhibitors are important in cancer and viral infections and are now considered an attractive drug target.[34b]

Likewise, carbonic anhydrase (CA), which includes zinc-dependent metalloenzymes, has been identified in human tissue, and their affinity as inhibitors and activators is associated with many vital activities. It plays fundamental role in many physiological and pathological events for all organisms and catalyzes the hydration reaction of CO_2, which results in bicarbonate and protons.[35] To date, 16 carbonic anhydrase isoforms have been identified, including CA I and CA II isoforms of the α-CA class in cytosolic form. These isoenzymes are associated with red blood cells, osteoclasts, gastrointestinal tract, eyes, lungs, brain, and testes and play a role in maintaining the physiological pH of the blood in red blood cells. Moreover, CA II is associated with various diseases, such as glaucoma, epilepsy, edema, renal tubular acidosis, altitude sickness, and osteoporosis.[35–38]

Two different new *N*-substituted carbazole zinc Pcs were synthesized herein, and their photophysical and photochemical properties and cyclic voltammograms were examined in dimethylformamide (DMF). The α-glucosidase in vitro inhibitory activities of compounds (**4a** and **6a**) and their ligands (**3**, **4**, **5**, and **6**) were

compared to the standard drug acarbose and evaluated. As the IC_{50} values of compounds (**4**, **4a**, **5**, and **6**) showed strong inhibitory activity, to understand the enzyme inhibition mechanism, a kinetic study was performed. These compounds were determined as competitive inhibitors for α-glucosidase, such as acarbose. However, the inhibitory effects of complexes and ligands on human erythrocytes carbonic anhydrase isoenzymes hCA I and II were investigated. When the inhibition results were compared to the reference inhibitor acetazolamide (AZA), it was observed that **4a** and **6a** had a very strong inhibitory effect on both isoenzymes. Furthermore, the inhibition potential of the **4a** and **6a** complexes was supported by molecular modeling studies.

2 | EXPERIMENTAL

2.1 | Materials

Carbazole, ethylene carbonate, potassium hydroxide (KOH), acetyl chloride (AcCl), zinc chloride ($ZnCl_2$), benzaldehyde, 4-nitrophthalonitrile, potassium carbonate (K_2CO_3), 1, 8-diazabicyclo[5.4.0]undec-7-ene (DBU), 1,3-diphenylisobenzofuran (DPBF), Zn $(OAc)_2.2H_2O$, DMF, methanol, ethanol, tetrahydrofuran (THF), and dichloromethane (DCM) were purchased from commercial suppliers. The solvents that were used in the study were appropriately distilled. Sodium sulfate (Na_2SO_4) was used for drying before the solvent was removed on a rotary evaporator under reduced pressure.

2.2 | Equipment

For ^{1}H NMR and ^{13}C NMR spectra, VARIAN Infinity Plus 300 MHz NMR spectrometer was used. Chemical shifts were expressed in ppm relative to $CDCl_3$ (d 7.26 and 77.0 for ^{1}H NMR and ^{13}C NMR, respectively) and tetramethylsilane as the internal standards. Infrared spectra were recorded on an Ati Unicam Mattson 1000 Series FT-IR (ATR system) spectrometer. Melting points were recorded on a Büchi B-540 apparatus. The MALDI-TOF spectra were recorded with Bruker Daltonics flexAnalysis. Purification of compounds was realized with column chromatography using silica gel 60 (40–63 μm, Fluka). Thin-layer chromatography (TLC) was performed on Merck 0.2 mm silica gel (60 F254 analytical aluminum plates). Photo-irradiation was conducted using a general electric quartz line lamp (300 W). UV–Vis spectra were obtained using Shimadzu UV 2600 model spectrophotometer. Fluorescence measurements were performed on Agilent Technologies Cary Eclipse spectrophotometer.

2.3 | Synthesis

2.3.1 | Synthesis of 2-(9H-carbazol-9-yl) ethan-1-ol (**1**)

Compound **1** was synthesized according to the literature.[39] Briefly, ethylene carbonate (1.05 g, 11.96 mmol) and K_2CO_3 (1.65 g, 11.96 mmol) were added to a stirred solution of carbazole (1 g, 5.98 mmol) in freshly distilled DMF (10 ml), and the mixture was refluxed for 8 h. After the completion and isolation of the reaction, compound **1** was obtained as a white solid by crystallizing it from ethanol. Yield: 1.02 g (81%). m.p. 80–82°C. FT-IR ν_{max} (cm^{-1}): 3203 (OH), 3049 (Ar-H), 2867 (aliphatic C-H), 1593 (C=C), 1451 (C-N), 1323 (C-H). ^{1}H NMR (300 MHz, $CDCl_3$): δ ppm = 8.10 (m, 2H), 7.47 (m, 2H), 7.42 (m, 2H), 7.26 (m, 2H), 4.46 (t, 2H, J = 5.3 Hz), 4.04 (t, J = 5.3 Hz, 2H). ^{13}C NMR (75 MHz, $CDCl_3$): δ ppm = 140.9, 126.1, 123.1, 120.6, 119.5, 109.2, 61.5, 45.6. Anal. Calcd. for $C_{14}H_{13}NO$ (%): C, 79.59; H, 6.20; N, 6.63. Found: C, 79.36; H, 6.34; N, 6.86.

2.3.2 | Synthesis of 2-(3-acetyl-9H-carbazol-9-yl)ethyl acetate (**2**)

Anhydrous $ZnCl_2$ (1.03 g, 7.57 mmol) was added to a stirring solution of 2-(9H-carbazol-9-yl)ethan-1-ol (**1**) (1 g, 4.73 mmol) in 50 ml of DCM, and the mixture was stirred under an N_2 atmosphere at 0°C for 30 min. Acetyl chloride (0.84 ml, 11.83 mmol) was injected using an injector. The reaction mixture was stirred under an N_2 atmosphere at room temperature for 3 h; then, 6 ml of 37% HCl and 4 ml of H_2O were added to the reaction and stirred at room temperature for 30 min. The mixture was then worked up (3 × 20 ml) with DCM. The organic phase was collected and dried with Na_2SO_4, and the solvent was removed in the evaporator. The residue was purified by DCM using silica gel column chromatography. After the fractions were collected, the collected fractions were crystallized from methanol and obtained as a white solid. Yield: 0.6 g (43%). m.p. 93–95°C. FT-IR ν_{max} (cm^{-1}): 3048 (Ar-H), 2,976 (aliphatic C-H), 1740 (C=O), 1664 (C=C), 1595 (C-N), 1262–1231 (C-H), 1039 (C-O-C). ^{1}H NMR (300 MHz, $CDCl_3$): δ ppm = 8.69 (m, 1H, H_3), 8.12 (m, 2H), 7.51 (m, 1H), 7.41 (m, 2H), 7.31 (m, 1H), 4.53 (t, J = 5.0 Hz, 2H, -CH_2-), 4.44 (t, J = 5.0 Hz, 2H, -CH_2-), 2.71 (s, 3H, -CO-CH_3), 1.90 (s, 3H, -CO-CH_3). ^{13}C NMR (75 MHz, $CDCl_3$): δ ppm = 197.9C_1', 171.0C_{15}, 143.5C_{11}, 141.2C_{12}, 129.4C_3, 126.9C_1, 126.7C_5, 123.5C_6, 123.0C_7, 122.1C_9, 120.9C_4, 120.7C_8, 109.3C_2, 108.5C_{10}, 62.2C_{14}, 42.1C_{13}, 27.0C_2', 21.0C_{16}. Anal. Calcd. for

$C_{18}H_{17}NO_3$ (%): C, 73.20; H, 5.80; N, 4.74. Found: C, 73.33; H, 5.54; N, 4.48.

2.3.3 | Synthesis of 1-(9-[2-hydroxyethyl]-9H-carbazol-3-yl)ethan-1-one (**3**)

Compound **3** was carried out according to the procedure described in the literature.[40] Briefly, 2-(3-acetyl-9H-carbazol-9-yl)ethyl acetate (**2**) (0.5 g, 1.69 mmol) was ammonolized with NH_3 (g) in absolute methanol (20 ml). The product (**3**) was obtained as colorless crystals by crystallizing it from absolute ethanol, yield: 0.39 g (91%). m.p. 164–166°C. FT-IR ν_{max} (cm^{-1}): 3396 (OH), 3051 (Ar-H), 2917–2865 (aliphatic C-H), 1653 (C=O), 1592 (C=C), 1438 (C-N), 1330–1252 (C-H). ^1H NMR (300 MHz, $CDCl_3$): δ ppm = 8.62 (d, J = 1.7 Hz, 1H, H_4), 8.13 (d, J = 7.7 Hz, 1H, $H_{aromatic}$), 8.04 (dd, J = 8.5, 1.8 Hz, 1H, $H_{aromatic}$), 7.49 (m, 2H, $H_{aromatic}$), 7.34–7.29 (m, 2H, $H_{aromatic}$), 4.49 (t, J = 6.3 H, 2H, -CH_2-), 4.10 (t, J = 5.0 Hz, 2H, -CH_2-), 2.59 (s, 3H). ^{13}C NMR (75 MHz, $CDCl_3$): δ ppm = 198.1C_1', 143.8C_{11}, 141.6C_{12}, 129.1C_3, 126.9C_5, 123.5C_1, 123.0C_6, 121.9C_7,C_9, 120.9C_4, 120.6C_8, 109.7C_2, 108.7C_{10}, 61.6C_{13}, 46.0C_{14}, 26.8C_3'. Anal. Calcd. for $C_{16}H_{15}NO_2$ (%): C, 75.87; H, 5.97; N, 5.53. Found: C, 76.01; H, 5.66; N, 5.69.

2.3.4 | Synthesis of 4-(2-(3-acetyl-9H-carbazol-9-yl)ethoxy)phthalonitrile (**4**)

To a stirred solution of 1-(9-[2-hydroxyethyl]-9H-carbazol-3-yl)ethane-1-one (**3**) (0.5 g, 1.97 mmol) in freshly distilled DMF (12 ml), 4-nitrophthalonitrile (0.41 g, 2.37 mmol) was added. Then, anhydrous K_2CO_3 (0.41 g, 2.96 mmol) was added and refluxed under an N_2 atmosphere at 70°C for 48 h. The completion of the reaction was followed by TLC. After the reaction was complete, the mixture was added dropwise to 200 ml of ice water and stirred. The precipitated solids were filtered, washed with plenty of water, and dried with Na_2SO_4. The brown solid was purified by silica gel column chromatography using DCM. The compound **4** were obtained as light-yellow solid. Yield: 0.32 g (43%). m.p. 232–234°C. FT-IR ν_{max} (cm^{-1}): 3074 (Ar-H), 2230 (C≡N), 1656 (C=O), 1595 (C=C), 1562 (C-N), 1255–1247 (C-H), 1104 (C-O-C). ^1H NMR (300 MHz, $CDCl_3$): δ ppm = 8.72 (s, 1H, H_3), 8.17–8.13 (m, 2H), 7.58–7.49 (m, 4H), 7.34 (m, 1H), 7.06 (d, J = 2.7, 1H), 6.98 (dm, J = 2.6 Hz, 1H), 4.80 (t, J = 5.2 Hz, 2H, -CH_2-), 4.47 (t, J = 5.0 Hz, 2H, -CH_2-), 2.74 (s, 3H). ^{13}C NMR (75 MHz, $CDCl_3$): δ ppm = 197.9C_1', 161.2C_{15}, 143.4C_{17}, 141.1C_{12}, 135.4C_3, 129.7C_5, 127.0C_1, 126.9C_6, 123.6C_9, 123.2C_7, 122.2C_4, 121.1C_8, 121.0C_{16},C_{20}, 119.5C_{19},C_{20}, 119.4C_{21},C_{22}, 109.2C_2, 108.5C_{10},C_{18}, 108.2C_{13}, 67.4C_{14}, 42.6C_{13}, 27.0C_2'. Anal. Calcd. for $C_{24}H_{17}N_3O_2$ (%): C, 75.98; H, 4.52; N, 11.08. Found: C, 75.71; H, 4.64; N, 10.95.

2.3.5 | Synthesis of zinc (II) phthalocyanine (**4a**)

To a stirring solution of 4-(2-(3-acetyl-9H-carbazol-9-yl) ethoxy)phthalonitrile (**4**) (0.1 g, 0.26 mmol) and Zn $(OAc)_2.2H_2O$ (0.07 g, 0.32 mmol) in fresh distilled DMF, one to two drops of DBU were added at 160°C. The mixture was stirred at the same temperature for 24 h under a nitrogen atmosphere. Following that, the temperature was brought to room temperature, poured into ice water (50 ml), then stirred and filtered. The filtrates were washed with plenty of water and hot ethanol, and the unreacted organic materials were removed. After drying in vacuo, it was purified by silica gel column chromatography using THF. Yield: 0.05 g (12%). m.p. > 300°C. FT-IR ν_{max} (cm^{-1}): 2955 (Ar-H), 2870–2851 (aliphatic C-H), 1666 (C=O), 1594 (C=C), 1361–1231 (C-H), 1055 (C-O-C). ^1H NMR (300 MHz, $CDCl_3$): δ ppm = 8.67 (m, 6H, H), 8.10 (m, 14H), 7.46 (m, 14H), 7.20 (m, 14H), 4.70(m, 8H), 4.37(m, 8H), 1.814 (bs, 12H). UV–Vis (DMF), λ_{max}, nm: 675, 607, 330, 321. MALDI-TOF mass spectrometry: m/z $[M]^+$ calcd. for $C_{96}H_{68}N_{12}O_8Zn$: 1583.06; found $[M+H]^+$ 1583.93. Anal. Calcd. for $C_{96}H_{68}N_{12}O_8Zn$ (%): C, 72.84; H, 4.33; N, 10.62. Found: C, 72.68; H, 4.42; N, 10.35.

2.3.6 | Synthesis of (E)-1-(9-[2-hydroxyethyl]-9H-carbazol-3-yl)-3-phenylprop-2-en-1-one (**5**)

1-(9-[2-hydroxyethyl]-9H-carbazol-3-yl)ethan-1-one (**3**) (1 g, 3.95 mmol) was dissolved in ethanol, and 15% KOH (13 ml) was added dropwise. After stirring for 30 min at room temperature, benzaldehyde (0.49 g, 4.06 mmol) dissolved in ethanol was added dropwise and stirred overnight at room temperature. The reaction mixture was precipitated in ice water, and the precipitated solid was filtered and dried under vacuum. The solid was purified by silica gel column chromatography using DCM. The product was obtained as a yellow solid. Yield: 1.05 g (91%). m.p 163–165°C. FT-IR ν_{max} (cm^{-1}): 3380 (OH), 3054 (Ar-H), 2937–2867 (aliphatic C-H), 1647 (C=O), 1597–1567 (C=C), 1436 (C-N), 1330 (C-H). ^1H NMR (300 MHz, $CDCl_3$): δ ppm = 8.74 (d, J = 1.5 Hz, 1H, H_3), 8.18–8.14 (m, 2H, $H_{aromatic}$), 7.83–7.64 (m, 4H), 7.53–7.43 (m, 5H), 7.33–7.28 (m, 2H), 4.51 (t, J = 5.3 Hz, 2H), 4.12

(m, 2H). ^{13}C NMR (75 MHz, $CDCl_3$): δ ppm = 189.6C_1', 143.9C_{11}, 141.6C_3', 135.4C_4', 130.5C_3, 129.8C_6',C_6", 129.2C_5',C_5", 128.7C_{12}, 127.1C_7', 126.9C_1, 123.5C_5, 123.1C_6, 122.3C_4,C_9, 122.2C_7, 121.0C_2', 120.6C_8, 109.7C_2, 109.0C_{10}, 61.6C_{13}, 46.1C_{14}. MALDI-TOF MS: m/z $[M]^+$ calcd. for $C_{23}H_{19}NO_2$: 341.41; found $[M + H]^+$ 341.55. Anal. Calcd. for $C_{23}H_{19}NO_2$ (%): C, 80.92; H, 5.61; N, 4.10. Found: C, 81.13; H, 5.44; N, 3.96.

2.3.7 | Synthesis of 4-(2-(3-cinnamoyl-9H-carbazol-9-yl)ethoxy)phthalonitrile (**6**)

(E)-1-(9-[2-hydroxyethyl]-9H-carbazol-3-yl)-3-phenylprop-2-en-1-one (**5**) (0.5 g, 1.46 mmol) and 4-nitrophthalonitrile (0.5 g, 2.93 mmol) were dissolved in fresh distilled DMF (12 ml). To the resulting mixture, anhydrous K_2CO_3 (0.3 g, 2.20 mmol) was added and refluxed under an N_2 atmosphere at 80°C for 96 h. After the reaction was complete, which was controlled with TLC, the mixture was purified according to the procedure described for **4** above. Compound **6** was obtained as a light-brown solid. Yield: 0.38 g (55%). m.p. 186–188°C. FT-IR ν_{max} (cm^{-1}): 3066 (Ar-H), 2951 (aliphatic C-H), 2231 (C≡N), 1649 (C=O), 1590 (C=C), 1491 (C-N), 1296–1219 (C-H), 1023 (C-O-C). ^{1}H NMR (300 MHz, $CDCl_3$): δ ppm = 8.78 (d, J = 1.5 Hz, 1H), 8.23 (dd, J = 8.5 Hz, J = 1.4 Hz, 1H), 8.16 (d, J = 7.6 Hz, 1H), 7.82 (q, J = 15.5 Hz, 3H), 7.56–7.50 (m, 4H), 7.47–7.42 (m, 3H), 7.35 (m, 1H), 7.5 (d, J = 2.7 Hz, 1H), 6.97 (dd, J = 8.5 Hz, J = 2.3 Hz, 1H), 4.78 (t, J = 5.3 Hz, 2H, -CH_2-), 4.46 (t, J = 5.3 Hz, 2H, -CH_2-). ^{13}C NMR (75 MHz, $CDCl_3$): δ ppm = 189.7C_1·, 161.2C_{15}, 144.3C_3', 143.4C_{11}, 141.1C_{19}, 135.4C_4·, 135.3C_3, 130.6C_{12}, 130.5C_7', 129.2C_6',C_6", 128.8C_5',C_5", 127.2C_1, 127.1C_5, 123.6C_6, 123.3C_4, 122.4C_9, 122.3C_7, 121.2C_2', 121.0C_8, 119.5C_{20}, 119.4C_{16}, 117.6C_{17}, 115.6C_{22}, 115.2C_{21}, 109.3C_2, 108.8C_{10}, 108.1C_{18}, 67.4C_{14}, 42.6C_{13}. Anal. Calcd. for $C_{31}H_{21}N_3O_2$ (%): C, 79.64; H, 4.53; N, 8.99. Found: C, 79.44; H, 4.78; N, 8.85.

2.3.8 | Synthesis of zinc (II) phthalocyanine (**6a**)

To a stirring solution of 4-(2-(3-cinnamoyl-9H-carbazol-9-yl)ethoxy)phthalonitrile (**6**) (0.1 g, 0.21 mmol) and Zn $(OAc)_2.2H_2O$ (0.06 g, 0.26 mmol) in fresh distilled DMF, one to two drops of DBU were added. The reaction was then stirred under a nitrogen atmosphere at 170°C for 24 h. After the reaction was complete, the mixture was purified according to the procedure described for **4a** above. Complex **6a** was obtained as a green solid. Yield: 0.06 g (14%). m.p. > 300°C. FT-IR ν_{max} (cm^{-1}): 2956 (Ar-H), 2867 (aliphatic C-H), 1646 (C=O), 1595 (C=C), 1484 (C-N), 1362–1232 (C-H), 1056 (C-O-C). ^{1}H NMR (300 MHz,DMSO-d_6): δ ppm = 7.89 (m, 17H, H), 7.75 (m, 17H), 7.43 (m, 21H), 7.25 (m, 21H), 4.89 (m, 8H), 4.51 (m, 8H). UV–Vis (DMF), λ_{max}, nm: 676, 613, 350. MALDI-TOF MS: m/z $[M]^+$ calcd. for $C_{124}H_{84}N_{12}O_8Zn$: 1935.49: Found $[M + H]^+$ 1935.39. Anal. Calcd. for $C_{124}H_{84}N_{12}O_8Zn$ (%): C, 76.95; H, 4.37; N, 8.68. Found: C, 77.12; H, 4.16; N, 8.51.

2.4 | Electrochemical study

Cyclic voltammogram studies of zinc (II) Pcs (**4a** and **6a**) were recorded on Gamry Interphase 1000 potentiostat using the following electrode system: glassy carbon as the working electrode, Pt disk as the reference electrode, and Pt wire as the counter electrode. The measurements in the study were carried out in DMF containing tetrabutylammonium hexafluorophosphate ($TBAPF_6$) as the supporting electrode. The Fc/Fc^+ redox couple was used as an external standard to calibrate the results. Complexes **4a** and **6a** (1 mM) were measured at scan rates of 50 to 150 mV s^{-1}.

2.5 | α-Glucosidase inhibitory enzymatic and kinetics assay

The inhibitory activities of the synthesized compounds (**3–6**, **4a**, and **6a**) were measured spectrophotometrically (using Shimadzu UV–Vis spectrophotometer) toward α-glucosidase (*Saccharomyces cerevisiae*; E.C3.2.1.20) using *p*-nitrophenyl α-*D*-glucopyranoside (4-pNPG) with some modifications according to the previously reported literature.[27,41] Each measurement was performed in potassium phosphate buffer (50 mM, pH 6.8) with 4-pNPG substrate (1 mM). The enzyme (20 µl, 0.1 U ml^{-1}) and inhibitor analog were preincubated for 3 min at 37°C, 200 rpm. The reaction was initiated by adding the substrate, then the mixture was incubated at 37°C for 1 min. The reaction was stopped by adding 0.2 M Na_2CO_3 (80 µl) to the medium and the released *p*-nitrophenol was measured at 405 nm. Both the synthesized compounds (**3–6**, **4a**, and **6a**) and acarbose (as control) were studied in triplicate ranging from 2 to 180 µM concentrations in buffer solution. The percent inhibition of α-glucosidase was calculated and IC_{50} values were found by drawing graphs.

The kinetics of α-glucosidase enzyme inhibition were investigated based on the preincubation and measurement times in the inhibition assay detailed above. Three different concentrations were used for each compound

whose inhibition kinetics were studied. Also, a substrate concentration in the range of 0.01–0.13 mM was used. SigmaPlot enzyme kinetics software version 14.0 was used to plot the Lineweaver–Burk and Hanes–Woolf, and *Ki* values of α-glucosidase inhibitors were determined by graph fitting analysis.[42]

2.6 | The inhibition assay for hCA I and II isoforms

The inhibitory effects of newly synthesized *N*-substituted carbazole zinc Pcs (**4a** and **6a**) and their ligands (**3**, **4**, **5**, and **6**) on hCA I and II isoenzymes were determined against the standard inhibitor AZA. The hCA I and II isoenzymes were isolated and purified from human erythrocytes using a sepharose-4B-L-tyrosine sulfanilamide affinity column at 280 nm, then checked using SDS-PAGE.[43] The amount of purified protein was measured according to the standard bovine serum albümin.[44] The esterase activity measurements were defined as in the known method.[45] This method is based on the hydrolysis of hCA isoforms to *p*-nitrophenyl acetate, *p*-nitrophenol, and acetic acid, and *p*-nitrophenyl acetate was used as the substrate. The formation of *p*-nitrophenol from *p*-nitrophenyl acetate in the esterase activity measurement method was monitored spectrophotometrically, with an increase in absorbance at 348 nm at 25°C for 3 min. After the purification of the isoenzymes, they were dialyzed against a 0.05 M *Tris*-SO_4 (pH 7.4) buffer overnight and then stored at −80°C as 1 ml preparations to be used in inhibition studies. The inhibition effects of the newly synthesized *N*-substituted carbazole zinc Pcs (**4a** and **6a**) and their ligands (**3**, **4**, **5**, and **6**) were determined by the IC_{50} value with minor modifications.[46] To determine the IC_{50} value of each complex and their ligands, hCA I and II activity measurements were performed using at least five different concentrations. The control activity of hCA I and II is assumed to be 100%. With the results of the measurements, graphs of the percentage activity against the inhibitor concentration were drawn for each molecule. From these graphs, the IC_{50} values of each molecule, which reduced the enzyme activity by half, were determined.

2.7 | Docking protocol

Docking studies were performed against the crystal structure of human carbonic anhydrase I (hCA I) and the crystal structure of human carbonic anhydrase II (hCA II). X-ray crystal structures were obtained from PDB Databank (www.rcsb.org/) with PDB ID 5GMM[47] and 2FW4[48] for hCA I and 3M98[49] and 5AML[50] for hCA II. Enzyme structures were prepared using the Maestro Protein Preparation Wizard.[51] The 3D structures of reference ligand AZA were downloaded from the PubChem database (https://pubchem.ncbi.nlm.nih.gov/). The most stable conformers of the entire ligands were obtained by using Gaussian 09 software[52] employing the semiempirical PM6 method in the implicit solvent of water with the conductor-like polarizable continuum mode method.[53] The molecular docking data were obtained by using the AutoDock Vina-based CB-Dock server.[54,55] The results of docking calculations were evaluated as Vina scores and docked pose. Maestro pose viewer was used to analyze the binding mode and enzyme–ligand interactions.

3 | RESULTS AND DISCUSSION

3.1 | Synthesis and characterization

The synthetic pathway of the novel compounds in the study is shown in Schemes 1−3. First, 2-(9H-carbazol-9-yl)ethan-1-ol (**1**) was synthesized by refluxing commercially available carbazole in dry DMF in the presence of K_2CO_3 and ethylene carbonate.[39] Then, 2-(3-acetyl-9H-carbazol-9-yl)ethyl acetate (**2**) was obtained in 43% yield through the acetate reaction with acetyl chloride (AcCl). The synthesized compound (**2**) was hydrolyzed in $NH_{3(g)}$/MeOH to obtain 1-(9-[2-hydroxyethyl]-9H-carbazol-3-yl) ethan-1-one (**3**) (91%).[40] Following that, a novel carbazole phthalonitrile derivative 4-(2-(3-acetyl-9H-carbazol-9-yl)ethoxy)phthalonitrile (**4**) was obtained by refluxing compound (**3**), K_2CO_3, and 4-nitrophthalonitrile in dry DMF at 70°C for 48 h (Scheme 1). Therefore, the synthesis of carbazole phthalonitrile containing acetate group (**4**) was carried out successfully.

(E)-1-(9-[2-hydroxyethyl]-9H-carbazol-3-yl)-3-phenyl-proα2-en-1-one (**5**) was synthesized in 91% yield by reacting compound (**3**), 15% KOH, and benzaldehyde in ethanol at room temperature. Compound **5** was obtained after the necessary purification was refluxed in a nitrogen gas atmosphere at 80°C for 96 h in the presence of K_2CO_3 and 4-nitrophthalonitrile in dry DMF. Therefore, the new chalcone group containing carbazole phthalonitrile (**6**) was produced by the method based on aromatic nucleophilic substitution (SNAr) (Scheme 2).

Finally, new peripheral carbazole-derived substituted zinc (II) Pcs (**4a** and **6a**) were obtained as a result of the cyclotetramerization reaction of phthalonitrile compounds (**4** and **6**) in freshly distilled DMF by refluxing with Zn $(OAc)_2.2H_2O$ and DBU (catalyst) in a nitrogen gas atmosphere, respectively (Scheme 3).

SCHEME 1 Synthesis of starting compounds **1**, **2**, **3**, and 4-phthalonitrile derivative **4**

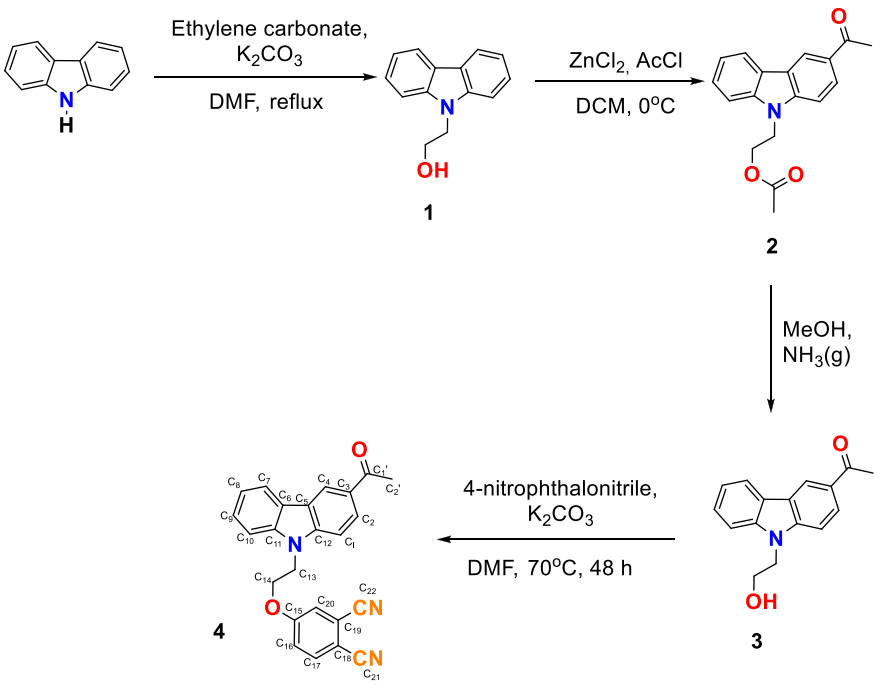

SCHEME 2 Synthesis of compound **5** and 4-phthalonitrile derivative **6**

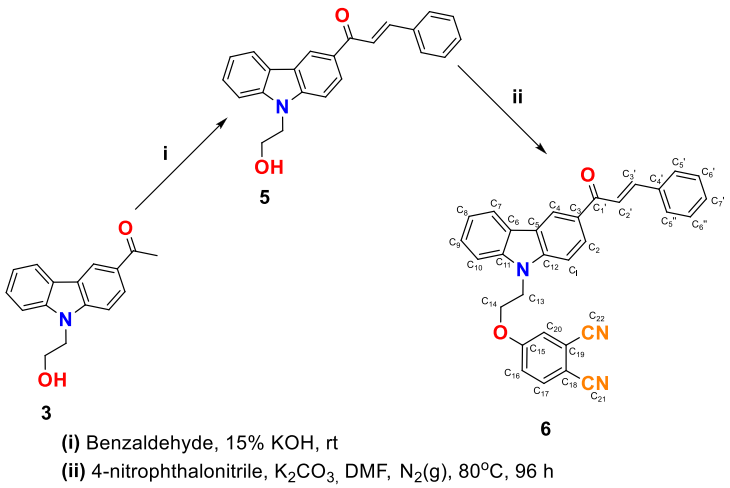

The structures of the new compounds were elucidated using spectroscopic methods, such as FT-IR, elemental analysis, UV–Vis, ^{1}H NMR, ^{13}C NMR, and MS. The infrared spectrum of **1** showed O-H at 3203, aromatic C-H at 3049, aliphatic C-H at 2867, aromatic C=C at 1593, and C-N at 1451 cm^{-1} with stretching vibrations (Figure S3). For the FT-IR spectrum of **2**, the disappearance of the peaks of the O-H group and the emergence of C=O stretching vibration around 1740 cm^{-1} confirms the formation of the compound (Figure S6). In the FT-IR spectrum of **3**, the O-H peak was observed at 3396 and the C=O peak at 1653 cm^{-1}, as expected (Figure S9). The FT-IR spectra of compound **5** appeared characteristic stretching vibrations of O-H group 3380 cm^{-1}, C=O group 1647 cm^{-1}, and alkene group (-C=C) 1597–1567 cm^{-1} (Figure S19). When the FT-IR spectra of phthalonitrile derivatives **4** and **6** are examined, the characteristic C≡N absorption bands to observe at 2230 and 2231 cm^{-1} prove the formation of these compounds (Figures S12 and S22). The disappearance of the stretching frequencies of C≡N groups in the FT-IR spectra of ZnPcs derivatives **4a** and **6a** is a strong indication that Pcs are formed by cyclotetramerization (Figures S15 and S25). When the UV–Vis spectra of complexes **4a** and **6a** were examined, it was observed that the metallophthalocyanines were similar to the Q bands and compatible with the D4h symmetry (Figures S14 and S24).[56]

In the ^{1}H NMR spectrum of 2-(9H-carbazol-9-yl) ethan-1-ol (**1**) in $CDCl_3$, the aromatic protons resonated as multiplets at 8.10, 7.47, 7.42, and 7.26 ppm,

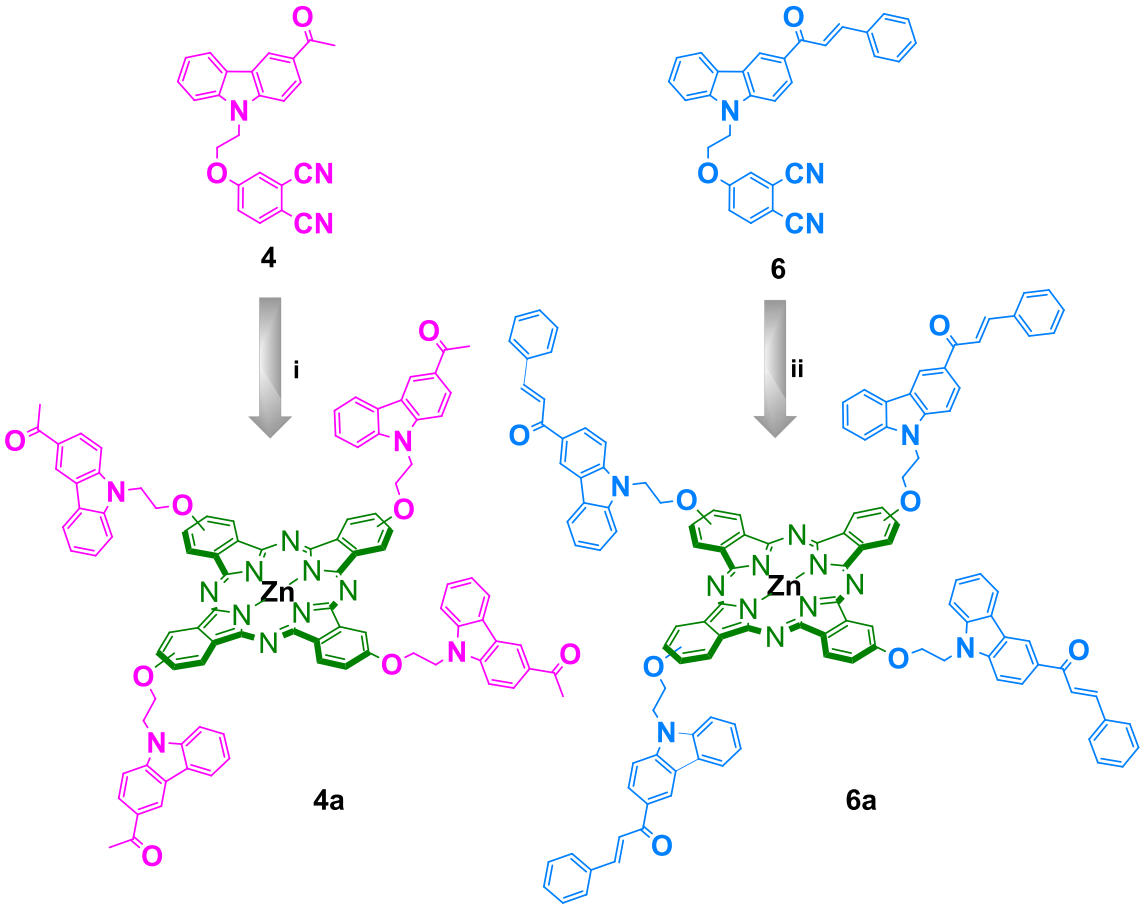

SCHEME 3 The preparation of Zn (II) Pcs (**4a** and **6a**) (i) DBU, Zn $(OAc)_2.2H_2O$, DMF 160°C, 24 h (ii) DBU, Zn $(OAc)_2.2H_2O$, DMF, 170°C, 24 h

respectively. The methylenic protons resonated as triplets at 4.46 ($J = 5.3$ Hz, 2H) and 4.04 ppm ($J = 5.3$ Hz, 2H). The eight signals in ^{13}C NMR indicated the symmetric structure. The acetylation reaction of the compound (**1)** resulted in 2-(3-acetyl-9H-carbazol-9-yl)ethyl acetate (**2**). The best evidence for the formation of compound **2** is the two methyl protons resonance signals (at 2.71 ppm as singlet for 3H and 1.09 ppm as singlet for 3H) in ^1H NMR and two carbonyl resonance signals at 197.9 and 171.0 ppm in ^{13}C NMR. The ammonolysis of compound **2** resulted in compound **3** by evidence of hydrolyzing of one acetate methyl group signal and one carbonyl group signal. The other resonance signals in ^1H NMR and ^{13}C NMR were resonated in deserved regions. To realize the target compound, the free hydroxy group in compound **3** was protected with 4-nitrophthalonitrile, which resulted in 4-(2-(3-acetyl-9H-carbazol-9-yl)ethoxy)phthalonitrile (**4**). In the ^1H-NMR spectrum of compound **4** in $CDCl_3$, the aromatic protons resonated in the expected region, whereas the methyleneic protons resonated between 4.80 and 4.47 ppm. Additionally, as compound **3** converts into compound **4**, the chemical shift sites of the methyleneic protons shift from 4.49–4.10 ppm to 4.80–4.47 ppm, which is a good indication. Moreover, 24 ^{13}C NMR resonance signals support the structure.

Although the configuration of Zn–phthalocyanine **4a** in the ^{13}C NMR is unclear due to aggregation or agglomeration, ^1H NMR shows the structure. In the ^1H NMR spectrum of complex (**4a**) in $CDCl_3$, the aromatic protons appeared at δ: 8.67, 8.10, 7.46, and 7.20 ppm as multiplets, respectively. However, the ^{13}C NMR of complex **4a** could not be measured, despite testing different deuterosolvents ($CDCl_3$, DMSO-d_6, CD_3OD, and pyridine-d_5).

However, compound (**5**), which formed during the reaction between compound **3** and benzaldehyde, resulted in (E)-1-(9-[2-hydroxyethyl]-9H-carbazol-3-yl)-3-phenylprop-2-en-1-one. This chalcone structure was elucidated by the ^1H NMR and ^{13}C NMR spectroscopic analyses. The most striking peak is the disappearance of the methyl peak in compound **5**, and the second most striking peak is the shift of the carbonyl group in compound **5** (189.6 ppm) to an area that is 9 ppm higher than that of compound **3** (198.1 ppm). The 23 lines in the ^{13}C NMR spectra supported the structure.

To arrive at compound **6**, the free hydroxyl group in compound **5** was protected with 4-nitrophthalonitrile. The NMR spectrum of compound **6** can be determined by comparing it with the spectrum of compound **5**. The most significant difference of compound **6** (resonated between 4.78 and 4.45 ppm) and compound **5** (resonated between 4.53 and 4.11 ppm) is the chemical shift values of the methylenic protons in the same deuterium solvent. Another obvious difference regarding the formation of the molecule in ^{13}C NMR is the ring carbon to which the oxygen at 160 ppm is attached. The other carbon atoms resonated in the expected region. The ^{1}H NMR spectrum of phthalocyanine **6a** gave broad resonance peaks due to aggregation or agglomeration, as shown in **4a** in DMSO-d_6. The aromatic and double-bond protons appeared at δ: 7.89, 7.75, 7.43, and 7.25 ppm as multiplets. Additionally, the methylenic protons that were bound to the ring resonated at 4.89 and 4.51 ppm. However, ^{13}C NMR of complex **6a** could not be performed as in **4a**, despite using different deuterosolvents ($CDCl_3$, DMSO-d_6, CD_3OD, and pyridine-d_5). MALDI-TOF mass spectra of compounds **4a**, **5**, and **6a** showed molecular ion peaks at m/z = 1583.93 $[M + H]^+$, 341.55 $[M + H]^+$, and 1935.39 $[M + H]^+$, respectively (Figure S13, S18, and S23).

3.2 | UV–Vis absorption and aggregation studies

The UV–Vis absorption spectra of Pcs are characterized by the determinant properties of the Q and B bands in the ground state of electronic spectra. When the absorption spectra of the Pcs in Figure 1 were examined, the Q band, which is where the transition from HOMO to LUMO (π–π*) occurred, was between 607 and 676 nm and the B band was between 320 and 350 nm. The position, density, and sharpness of the Q band are the most important parameters in the application of Pcs. The Q band is affected by the metal in the center of phthalocyanine, solvents, and peripheral and non-peripheral substitution.[57] Since there is no absorption of carbazole in this region, this peak in the Q band belongs to phthalocyanine.

In this study, the absorption spectra of both **4a** and **6a** Pcs are investigated in various polar solvents, such as DMF, DMSO, THF, and DCM (Figure 1). The excellent solubility of Zn (II) Pcs **4a** and **6a** in these organic solvents was achieved by adding substituents to the carbazole ring system. Although complexes **4a** and **6a** did not show aggregation in DMF, DMSO, and THF, they showed little aggregation in DCM (Figure 1a and b).

The Q band spectra of **4a** and **6a** in DMF showed monomeric behavior, as evidenced by the single narrow Q band in metallophthalocyanine complexes.[58] For Zn (II) Pcs (**4a** and **6a**), whose aggregation behaviors were investigated in various solvents, DMF was recorded as the solvent that offers the most appropriate solubility. In addition, it has been selected for photochemical property studies. Concentration, complex metal ions, temperature, substituents, and solvents cause aggregation, which is the main problem for Pcs.[59,60] Therefore, the aggregation behavior of synthesized Zn (II) phthalocyanine complexes (**4a** and **6a**) was investigated at different concentrations in DMF (Figure 2). For both Pcs at concentrations ranging from 2×10^{-6} to 1.2×10^{-5} M, it did not show any aggregation, following the Lambert–Beer law. The linear relationship between absorbance and concentration, as shown in Figure 2a and b, proves that it does not show aggregation in the concentration range studied.

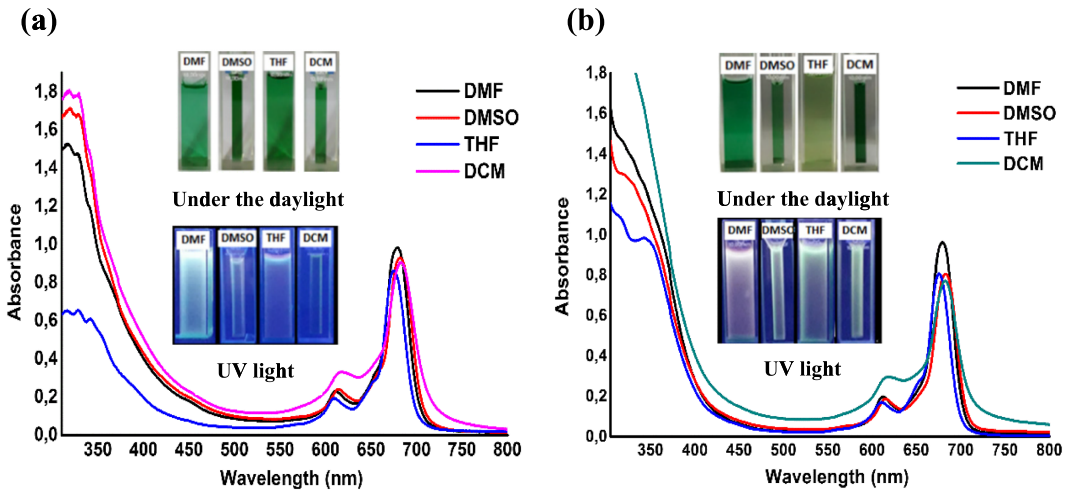

FIGURE 1 UV–Vis absorption spectra of (a) **4a** and (b) **6a** in various solvents at a concentration of 1.0×10^{-5} M

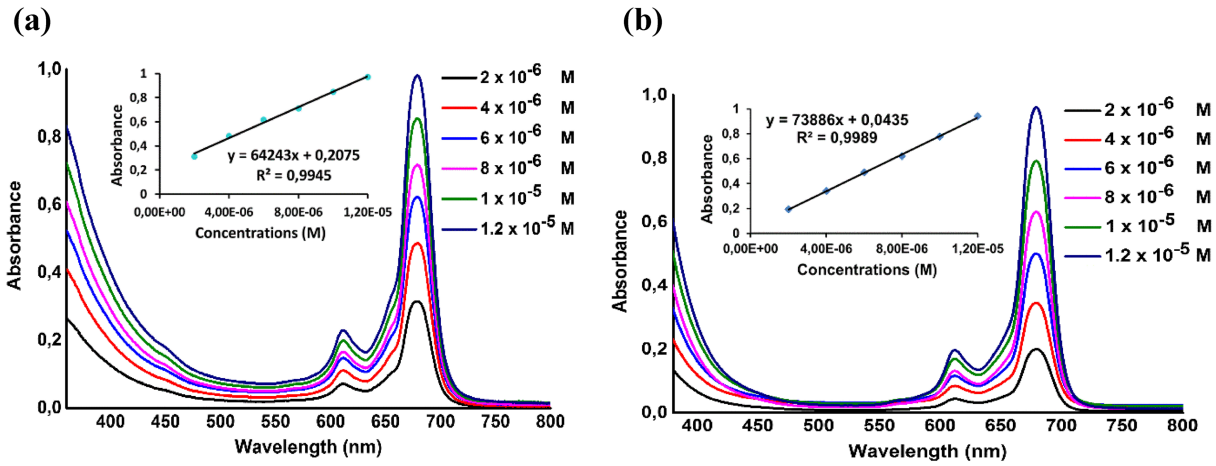

FIGURE 2 Aggregation behavior of (a) **4a** and (b) **6a** complexes in DMF at concentrations ranging from 2×10^{-6} to 1.2×10^{-5} M

3.3 | Fluorescence spectra

The fluorescence measurements were investigated in DMF, which provides the best resolution for both molecules. The fluorescence excitation and emission spectra of the new Pcs **4a** and **6a** are displayed in Figures S26 and 3. The excitation spectra of the examined zinc (II) phthalocyanine (**6a**) are similar to their absorption spectra (Figure 3). The proximity of the Q band maxima of the absorption and excitation spectra verifies that the molecule that is absorbing is the same one that is emitting. It is, therefore, understood that the absorption spectra are mirror images of the emission spectra, which show that the studied **4a** and **6a** phthalocyanine molecules did not show any degradation in the DMF during the excitation process.[21]

The fluorescence excitation, emission, and absorbance values of tetra-substituted peripherally carbazole-fused phthalocyanine derivatives (**4a** and **6a**) in DMF are summarized in Table 1. The characteristic absorption values in the Q band region of the complexes are shown at 675 nm (log $\varepsilon = 4.96$) for **4a** and 676 nm (log $\varepsilon = 4.98$) for **6a**. The stokes shift values of the **4a** and **6a** complexes in DMF are 9 and 14 nm, respectively (Table 1). Both of the stokes shift values are generally compatible with the phthalocyanine values.[62,63] The **4a** zinc (II) complex is relatively close to the standard ZnPc (6 nm) stokes shift value.

3.3.1 | Fluorescence quantum yields (Φ_F)

The fluorescence quantum efficiency (Φ_F), which measures the efficiency of a photophysical process, was quantified as the ratio of the number of photons that are

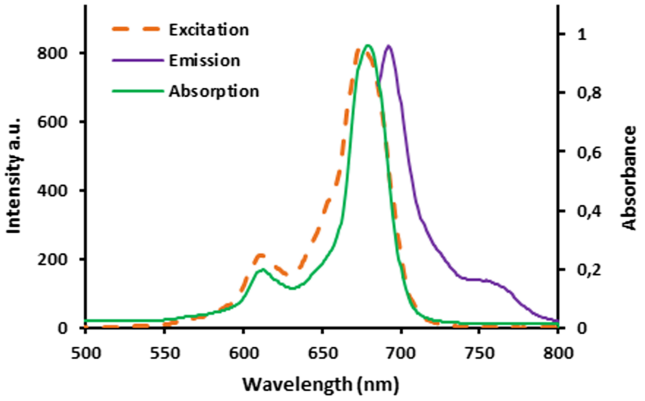

FIGURE 3 Absorption, emission, and excitation spectra of the **6a** complex in DMF at excitation wavelength 676 nm

emitted to the number of photons that are absorbed.[62] The fluorescent quantum yields (Φ_F) of all complexes (**4a** and **6a**) were measured in DMF by following a method as described in the literature,[64] and the results are provided in Table 2. The Φ_F value for **4a** was 0.06, and for **6a,** 0.13 showed the greatest value. The Φ_F values of these complexes are lower compared to the standard ZnPc (0.17),[64] which can be explained as the effect of the substituted groups on the phthalocyanine ring.

3.3.2 | Fluorescence quenching studies of 1,4-benzoquinone

The fluorescence quenching studies of benzoquinone (BQ) are realized because of the reaction that is formed by the energy transfer between zinc Pcs and BQ molecules. This is because the lowest excited state energy of

TABLE 1 Absorption and fluorescence data of **4a**, **6a**, and standard studied ZnPc

Compound	Solvent	Q band λ_{max} (nm)	log ε	Excitation λ_{Ex}, (nm)	Emission λ_{Em}, (nm)	Stokes shift (nm)
4a	DMF	675	4.96	674	683	9
6a	DMF	676	4.98	676	690	14
ZnPc[a]	DMF	670	5.37	670	676	6

[a]Data from Çamur et al (2012).[61]

TABLE 2 Photochemical, photophysical, and fluorescence quenching parameters of **4a** and **6a** in DMF

Compound	Φ_F	Φ_Δ	Φ_d ($\times 10^{-4}$)	Ksv (M^{-1})
4a	0.06	0.41	0.82	36.18
6a	0.13	0.12	0.40	77.43
ZnPc[a]	0.17	0.56	0.23	57.60

[a]Data from Zorlu et al. (2010).[64]

BQ is greater than the excited singlet state energy of zinc Pcs.[65,66] The decreasing emission spectra of the studied complexes in the presence of the increasing BQ concentration from 0 to 40 × 10^{-3} M are shown in Figure S27 for **4a** and Figure 4a for **6a**.

The fluorescence quenching experiment for ZnPcs (**4a** and **6a**) was performed in DMF according to the literature.[67] The fluorescence spectra of Zn (II) Pcs were recorded in the presence of different BQ concentrations, and the changes in the fluorescence intensity of these Pcs were determined according to the Stern–Volmer equation, as shown in equation 1.[68]

$$I_0/I = 1 + K\text{sv}[BQ], \quad (1)$$

where I_0 and I are the fluorescence intensities of fluorophore in the absence and presence of quencher, respectively; BQ is the concentration of the quencher, and Ksv is the Stern–Volmer constant.

The quenching mechanism can be considered dynamic since no changes were observed in the wavelengths and peaks of the emission bands in both complexes. The graph in Figure 4b for the two complexes (**4a** and **6a**) provides straight lines and is in accordance with the Stern–Volmer kinetics, which shows diffusion-controlled quenching mechanisms. The Ksv (Stern–Volmer equation) values for the BQ quenching of Zn (II) Pcs were determined by the slope of the graphs in Figure 4b, and these values are listed as 36.18 M^{-1} for the **4a** complex and 77.43 M^{-1} for **6a** in Table 2. The Ksv value of ZnPc **4a** was low compared to unsubstituted zinc (II) phthalocyanine, whereas **6a** was higher.

3.4 | Photochemical parameters

3.4.1 | Singlet oxygen quantum yields

The PDT technique, which is used in cancer treatment, produces singlet oxygen ($^1O_2$) with the energy transfer between the triple state of the photosensitizers and the ground state molecular oxygen, and the produced singlet oxygen is determined by the singlet quantum yield (Φ_Δ).[69] The singlet oxygen quantum yield was carried out according to equation 2.[67]

$$\Phi_\Delta = \Phi_\Delta^{Std} \frac{R \cdot I_{abs}^{Std}}{R^{Std} \cdot I_{abs}}, \quad (2)$$

where Φ_Δ^{Std} is the singlet oxygen quantum yields for the standard ZnPc ($\Phi_\Delta^{Std} = 0.56$ in DMF)[64,70] DPBF photobleaching rates of the respective samples (**4a** and **6a**) and standard are expressed as R and R^{Std}, respectively. Also, the light absorption rates of the respective samples (**4a** and **6a**) and the standard are expressed as I_{abs} and I_{abs}^{Std}, respectively. The light intensity used for Φ_Δ determinations was found to be 8.15×10^{15} photons s^{-1} cm^{-2}.

In this study, the singlet oxygen quantum yield values for the investigated zinc (II) Pcs (**4a** and **6a**) were determined in DMF. The absorption decays of DPBF, which is a singlet oxygen quencher, were monitored using the UV–Vis spectrometer at 417 nm. During the Φ_Δ determinations of the examined zinc (II) Pcs, no change in the Q-band intensities was observed. This means that the studied Pcs did not degrade during single oxygen measurements (Figure 5 for **4a** and **6a**).

The calculated Φ_Δ values of zinc (II) Pcs (**4a** and **6a**) and the Φ_Δ value of the standard zinc (II) Pc for comparison are summarized in Table 2. The quantum yields of singlet oxygen are affected by many factors, such as the magnitude of the substituents, the solvent's ability to quench single oxygen, the ground state of oxygen, the triple excited state lifetime, and the efficiency of energy transfer between the triple excited state.[71] The singlet oxygen quantum yield values of carbazole-derived Zn (II) Pcs ($\Phi_\Delta = 0.41$ for **4a** and $\Phi_\Delta = 0.12$ for **6a**) were

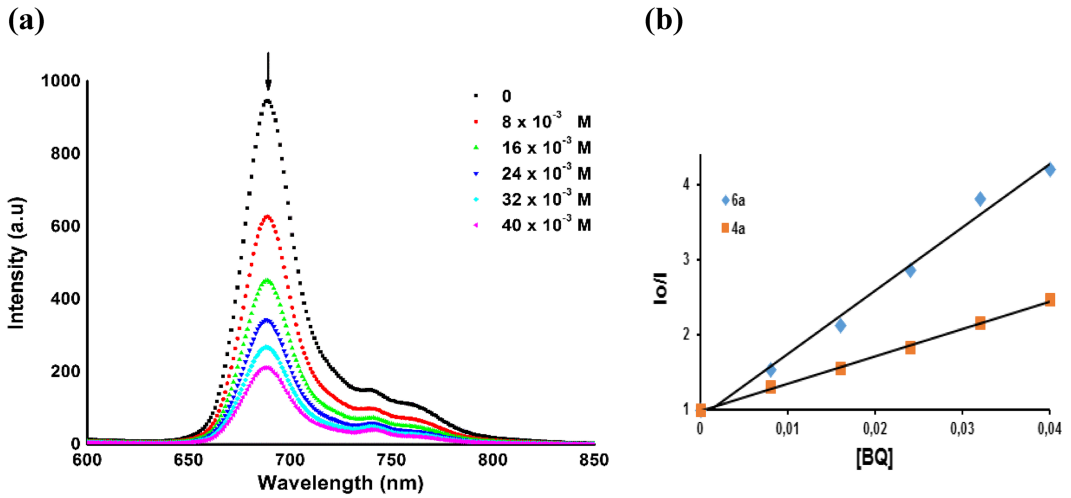

FIGURE 4 (a) Fluorescence emission spectral changes as a result of adding different BQ concentrations in DMF to the **6a** (1.0×10^{-5} M) complex (b) Stern–Volmer plot of **4a** and **6a** quenched with BQ ([***BQ***] = 0, 0.008, 0.016, 0.024, 0.032, and 0.040 M)

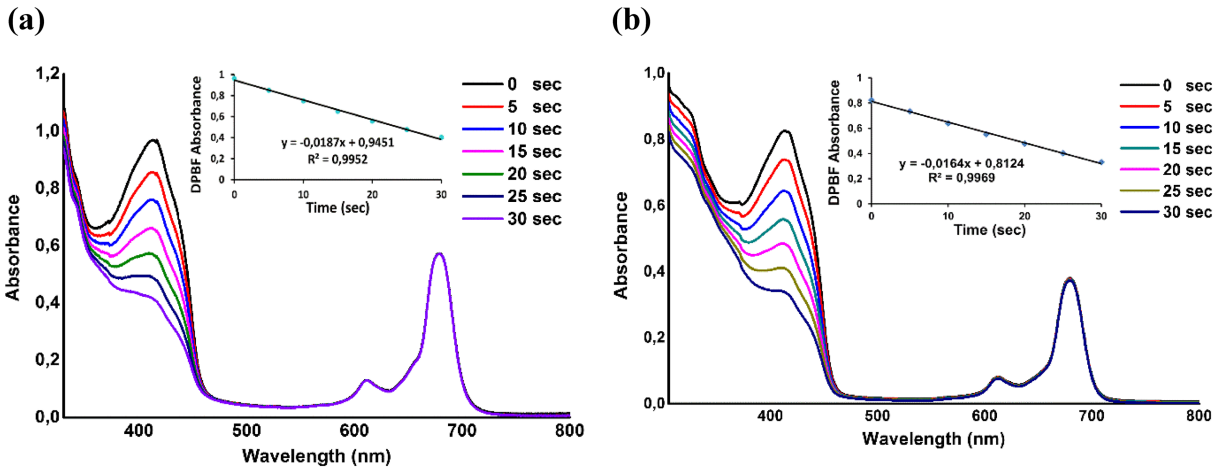

FIGURE 5 Singlet oxygen UV–Vis spectra with DPBF at a different time of complexes (a) **4a** and (b) **6a** in DMF at a concentration of 1×10^{-5} M

lower than the standard ZnPc ($\Phi_\Delta = 0.56$). When the peripheral-substituted MPcs **4a** and **6a** were compared, **4a** showed a higher Φ_Δ value. The **4a** complex is thought to have sufficient singlet oxygen production for PDT applications, even though the Φ_Δ value is lower than the standard ZnPc.[72]

3.4.2 | Photostability studies

For a molecule to be used as a photosensitizer, it is necessary to determine its stability behavior, that is, the quantum efficiency of photodegradation (Φ_d).[62] The photodegradation quantum yield (Φ_d) was carried out according to equation 3.[67]

$$\Phi_d = \frac{(C_0 - C_t).V.N_A}{I_{abs} \cdot S.\ t}, \quad (3)$$

where C_0 and C_t are the samples (**4a** and **6a**) concentrations before and after irradiation respectively, V is the reaction volume, N_A is the Avogadro constant, S is the irradiated cell area, t is the irradiation time, and I_{abs} is the overlap integral of the radiation source light intensity and the absorption of the samples (**4a** and **6a**).[67,71] Light intensity of 3.26×10^{16} photons s^{-1} cm^{-2} was used to determine this photodegradation parameter.

The determination of Φ_d is particularly important for photocatalytic reactions and biological applications, such as PDT. A photodegradation study of Zn (II) Pcs (**4a** and **6a**) was performed by observing a decrease in the

intensity of the absorption bands under light illumination in DMF (Figure 6 for both complexes).

According to the results, which are summarized in Table 2, the photodegradation quantum yields of new Zn (II) phthalocyanine complexes were 0.82×10^{-4} for **4a** and 0.4×10^{-4} for **6a**. As shown in the literature, stable Pcs show Φ_d values as low as 10^{-6}, whereas unstable Pcs show approximately 10^{-3}.[73] The Φ_d results of the investigated zinc (II) Pcs (**4a** and **6a**) are roughly similar when compared to the standard ZnPc. Additionally, the peripheral-substituted zinc (II) phthalocyanine molecule **6a** showed a lower Φ_d value according to the other peripheral zinc (II) phthalocyanine derivative **4a**, which demonstrates that **6a** is a more stable complex. As a result, the photostability of our two newly synthesized molecules (**4a** and **6a**) is moderate. For PDT applications, very unstable molecules cannot stay in the body for a long time because they degrade quickly. In addition, molecules that are highly stable for these applications cannot be easily destroyed by the host organism since they remain in the body for a long time.[64] Based on this information, the carbazole-derived ZnPcs (**4a** and **6a**), which we synthesized in this study, are suitable for PDT.

3.5 | Electrochemical characterization of the 4a and 6a

Pcs, which have an 18-electron aromatic system, lose one or two electrons in an oxidation state and gain one to four electrons in the case of reduction.[74] Zn (II) Pcs, which have a redox inactive metal center, show only phthalocyanine-based reduction and oxidation.[75] To examine the redox behavior of ZnPcs **4a** and **6a**, we performed an electrochemical study using a DMF/$TBAPF_6$ electrolyte system on a glassy carbon working electrode with the cyclic voltammogram technique. The cyclic voltammetry graph of the examined **4a** and **6a** complexes in the scanning range of 50–150 mV s^{-1} is shown in Figure 7a and b. One Pc-based reduction and one Pc-based oxidation within the potential window of the $TBAPF_6$/DMF electrolyte for both ZnPcs are observed (Figure 7a and b). According to the literature, it is expected that carbazole, which has an electron-donating structure, modulates the HOMO level by showing a significant effect in the anodic region.[76] Therefore, an irreversible oxidation process was observed in the study because cation formation occurred at more positive potentials for both molecules. The peak currents increased linearly on a cyclic voltammetry plot of scan rates ranging from 50 to 150 mV s^{-1} for these ZnPcs in Figure 7a and b, and this linearity indicates that the redox process is diffusion controlled.[77] In addition, this linearity is confirmed by showing the square root plot of peak current versus scan rate in Figure 7c for **4a** and Figure 7d for **6a**.

All results of ZnPcs (**4a** and **6a**) determined by voltammogram analysis are given in Table 3. According to the results, it showed an irreversible oxidation potential of 0.98 and 0.73 V and reversible reduction potential of −1.04 and −1.02 V for **4a** and **6a** at a scanning rate of 150 mV s^{-1}. Also, the HOMO energies of these two molecules (**4a** and **6a**) are −5.42 and −5.17 eV, and the LUMO energies −3.66 and −3.42 eV, respectively. Changes in electron density during electron donation or electron withdrawal by the substituents in the molecules (**4a** and **6a**) can shift the relative positions of the HOMO and LUMO levels.[74]

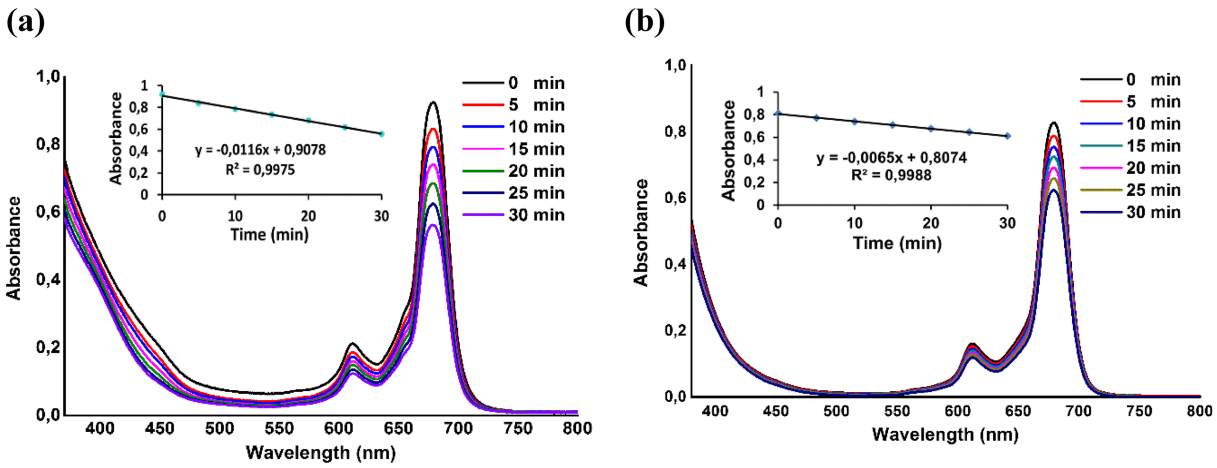

FIGURE 6 Photodegradation of (a) **4a** and (b) **6a** complexes in DMF at a concentration of 1×10^{-5} M. (inset: plot of Q band absorbance versus time)

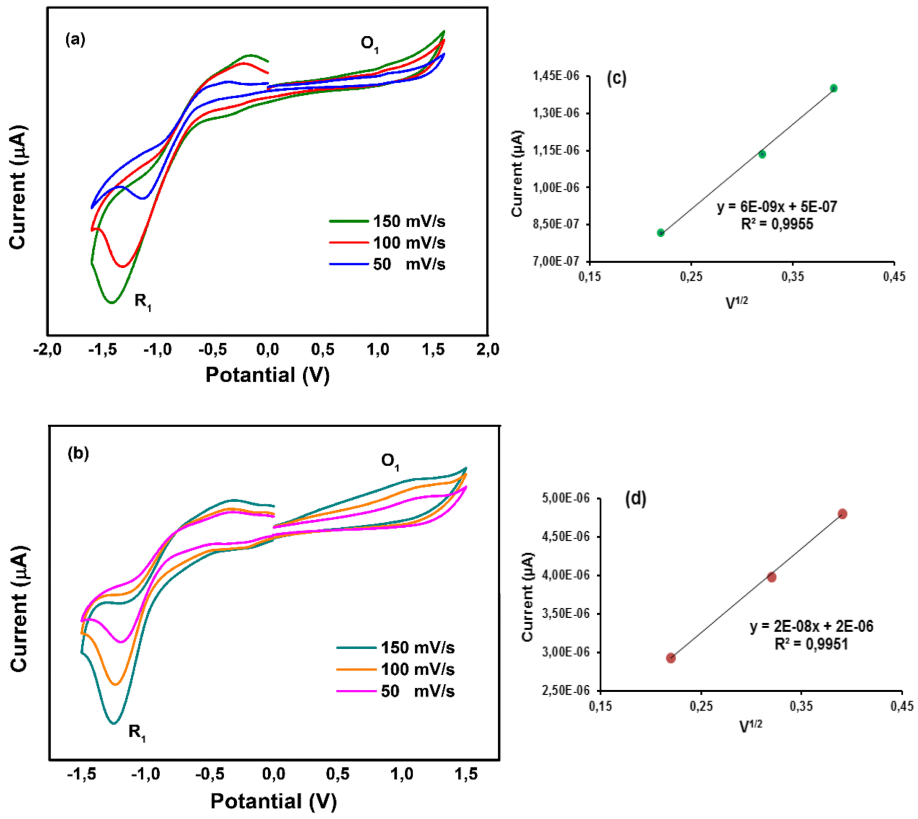

FIGURE 7 Cyclic voltammograms of ZnPc (a) **4a** and (b) **6a** recorded at scan rates (50–150 mV s^{-1}) in DMF containing 0.1 M $TBAPF_6$, (c) A plot of scan rates against versus peak current for **4a** and (d) for **6a**

TABLE 3 Electrochemical properties of **4a** and **6a**

Dye	λ_{max} (nm)	λ_{onset} (nm)	$E_{o\text{-}o}$ (eV)[a]	E_{red} (V)	E_{ox} (V)	$E_{HOMO/LUMO}$ (eV) [b,c]
4a	681	704	1.76	−1.04	0.98	−5.42/ −3.66
6a	682	707	1.75	−1.02	0.73	−5.17/ −3.42

[a]Bandgap ($E_{0\text{–}0}$) was calculated from the absorption onset wavelength (λ_{onset}) using $E_{0\text{–}0} = 1240/\lambda_{onset}$.
[b]HOMO level was calculated by the equation HOMO $= -(4.8 + E_{1/2})$ (vs. Fc/Fc^+).[78]
In this equation, 4.8 eV is the energy level of the ferrocene/ferrocenium couple below the vacuum level.
[c]LUMO level was estimated from $E_{LUMO} = E_{HOMO} + E_{0\text{–}0}$.[79a]

TABLE 4 α-Glucosidase inhibitory activities IC_{50} and K_i values of the tested compounds

Compounds	IC_{50} (µM)	Ki (µM)	R^2	Inhibition type
3	126.58 ± 3.48	132.55	0.9668	Competitive
4	8.62 ± 0.34	5.90	0.9098	Competitive
5	38.32 ± 1.13	35.70	0.9649	Competitive
6	7.54 ± 0.51	5.81	0.9650	Competitive
4a	47.86 ± 2.48	44.27	0.9710	Competitive
6a	62.59 ± 1.43	61.02	0.9854	Competitive
Acarbose*	55.58 ± 1.52	57.15	0.9685	Competitive[80]

[a]Acarbose was used as a control compound.

3.6 | α-Glucosidase inhibition results and kinetic characterization

The inhibitory activities of the Zn (II) phthalocyanine complexes (**4a** and **6a**) and their ligands (**3**, **4**, **5**, and **6**) were examined toward the α-glucosidase at the optimum pH for the first time by using the appropriate substrate (PNPG) (*p*-nitrophenyl-α-D-glucopyranoside), and the IC_{50} results and Ki values obtained are given in Table 4. Compounds **3** and **6a** showed a low inhibitory activity

compared to acarbose, whereas compounds **4**–**6** and **4a** showed a high inhibitory effect with IC_{50} values ranging from 7.54 ± 0.51 to 47.86 ± 2.48 μM. Compound **4** exhibited about seven times more potent inhibition activity than standard acarbose (55.58 ± 1.52 μM) with 8.62 ± 0.34 μM. Likewise, compound **6**, exhibited about eight times more potent inhibition activity than standard acarbose (55.58 ± 1.52 μM) with 7.54 ± 0.51 μM. These findings showed that carbazole phthalonitrile compounds (**4** and **6**) had higher inhibitory effects. It is known that compounds containing groups, such as nitrile and benzonitrile, are used in therapeutic applications because they show strong effects against glucosidase.[79b] It can be said that nitrile groups in compounds **4** and **6** have positive effects on the α-glucosidase enzyme due to their electron-withdrawing property. In addition, the strong inhibition activity of compound **6** display compared to other compounds can be explained by the fact that it contains chalcone and nitrile groups with electron-withdrawing features. Subsequently, compound **3** exhibited lower inhibition activity than the standard acarbose (55.58 ± 1.52 μM) with 126.58 ± 3.48 μM, whereas compound **5** exhibited strong inhibition activity than standard acarbose (55.58 ± 1.52 μM) with 38.32 ± 1.13 μM. On the other hand, Zn (II)phthalocyanine **4a** and **6a** (IC_{50} = 47.86 ± 2.48 μM for **4a** and IC_{50} = 62.59 ± 1.43 μM for **6a**) showed moderate inhibitory activity relative to standard acarbose (55.58 ± 1.52 μM). Substituent groups depending on the structure of Pcs in the peripheral position affect the inhibition activity.[79c] Different substituents in **4a** and **6a** Pcs exhibited different effects by interacting with the hydrophobic region through multiple modes.

Chalcones can potentially be used to inhibit or delay the action of the enzyme α-glucosidase against hyperglycemia. Moreover, they can cause several conformational changes in the enzyme through hydrogen bonding (π–π stacking interaction) by providing a hydrophobic environment and interaction.[79d] Therefore, we can explain why chalcone-containing compounds (**5** and **6**) show better activity than acetate-containing compounds (**3** and **4**), whereas chalcone substituent (**6a**) phthalocyanine shows lower activity than acetate-substituted carbazole phthalocyanine. Barut et al. reported peripheral tetra-[4-(9H-carbazol-9-yl)phenoxy]-substituted cobalt (II) and manganese (III) Pcs IC_{50} values for α-glucosidase of 25.93 ± 1.29 μM and 26.57 ± 2.67 μM, respectively.[20] Moreover, our peripheral carbazole Zn (II) phthalocyanine IC_{50} values were high.

Kinetic analysis of the compounds was performed to obtain information about the inhibitory mechanism of α-glucosidase. Kinetic graphs were obtained using SigmaPlot enzyme kinetic software version 14.0. Lineweaver–Burk and Hanes–Woolf plots of phthalonitrile derivatives (**4** and **6**) and Pcs (**4a** and **6a**) are shown in Figure 8, and that of other compounds (**3**, **5**, and acarbose) are shown in Figure S28. Based on the curve-fitting analysis, the compounds exhibited a competitive mechanism of inhibition against α-glucosidase, such as acarbose, which was used as the standard (Figure 8). The *Ki* values were calculated using these kinetic plots and are summarized in Table 4. *Ki* values of the compounds were determined in the range of 5.81 μM (R^2: 0.9650)–132.55 μM (R^2: 0.9668). With *Ki* values obtained, compounds **4** (5.90 μM, R^2: 0.9098) and **6** (5.81 μM, R^2: 0.9650) exhibited stronger inhibition. This means that **4** and **6** bind more strongly with the α-glucosidase substrate complex. The α-glucosidase inhibition constant (*Ki*) values of the compounds and acarbose are in the following order: **6** (5.81 μM, R^2: 0.9650) < **4** (5.90 μM, R^2: 0.9098) < **5** (35.70 μM, R^2: 0.9649) < **4a** (44.27 μM, R^2: 0.9710) < **acarbose** (57.15 μM, R^2: 0.9685) < **6a** (61.02 μM, R^2: 0.9854) < **3** (132.55 μM, R^2: 0.9668). The *Ki* results obtained were consistent with the enzyme activity results.

3.7 | Inhibition activity studies on hCA I and hCA II isoenzymes

In this study, the inhibitory effects of synthesizing two different new *N*-substituted carbazole zinc Pcs (**4a** and **6a**) and their ligands (**3**, **4**, **5**, and **6**) on the activity of hCA I and hCA II izoenzymes were examined under in vitro conditions. The inhibitory effects of the molecules were determined by the IC_{50} (inhibitor concentration that reduces the activity of the enzyme to half) value. AZA was used as the reference inhibitor. A low IC_{50} value indicates a strong inhibitory effect. In this study, IC_{50} values of **3**, **4**, **5**, **6**, **4a**, and **6a** for hCA I were found as 16.27 μM, 2.25 μM, 10.45 μM, 5.0 μM, 140.0 nM, and 116.60 nM, respectively (Table 5). According to these results, the **6a** molecule showed a very strong inhibition effect on hCA I activity. The inhibitory power of both **4a** and **6a** for hCA I was found to be very strong compared to AZA (Figure 10). Although **3** molecules showed the weakest inhibition effect for hCA I, the inhibition effect of **3** and **5** ligands was lower than that of **4** and **6** ligands. According to the IC_{50} values of the compounds, the inhibitory potentials against hCA I are listed as follows: **6a>4a>AZA>4>6>5>3**. On the other hand, for hCA II, IC_{50} values of **3**, **4**, **5**, **6**, **4a**, and **6a** were found to be 15.91 μM, 6.796 μM, 12.96 μM, 8.433 μM, 141.84 nM, and 362 nM, respectively (Table 5). In this case, the inhibition powers of these molecules are listed as follows: **4a>6a>AZA>4>6>5>3**. Although **4a** was the strongest inhibitor for hCA II, the inhibitory power of **4a** and **6a**

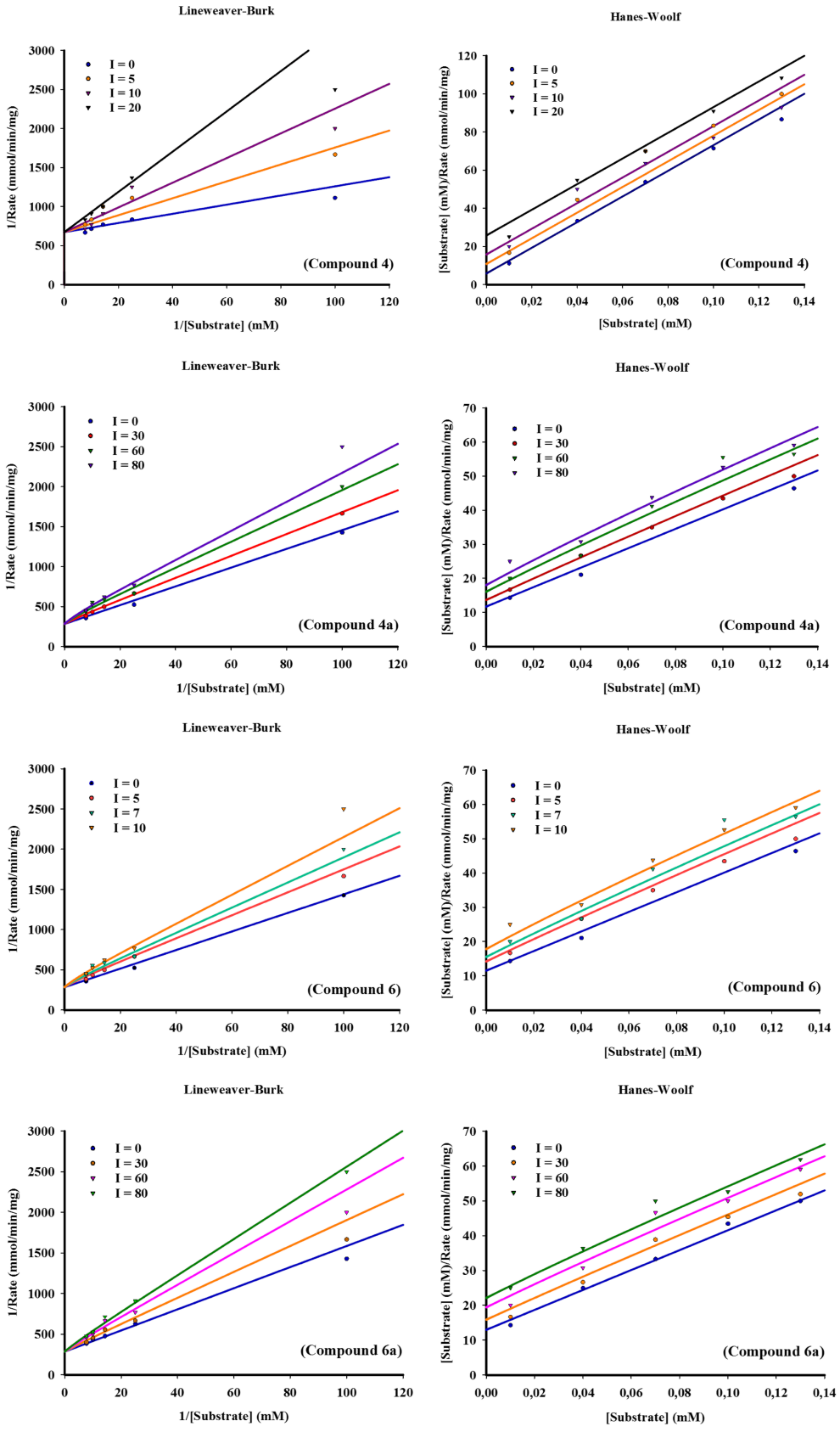

FIGURE 8 Lineweaver–Burk and Hanes–Woolf plots at different competitive type inhibitor concentrations for compounds **4**, **4a**, **6**, and **6a**

was higher than that for AZA. IC_{50} values of the **3**–**6**, **4a**, **6a**, and **AZA** for hCA I and hCA II are given comparatively (Figure 9). IC_{50} graphs of **4a** and **6a** molecules for hCA I and hCA II are shown in Figure 10, and the inhibition results of **3**–**6**, **4a**, and **6a** molecules on hCA I and hCA II are summarized in Table 5.

TABLE 5 The inhibition results of **3–6**, **4a**, and **6a** molecules on hCA I and hCA II

	For hCA I		For hCA II	
Compounds	IC_{50}	R^2	IC_{50}	R^2
3	16.27 μM	0.9208	15.91 μM	0.9909
4	2.25 μM	0.9402	6.796 μM	0.9762
5	10.45 μM	0.9739	12.96 μM	0.9704
6	5.0 μM	0.9899	8.433 μM	0.9599
4a	140.0 nM	0.9402	141.84 nM	0.9257
6a	116.60 nM	0.9817	362 nM	0.9069
AZA	462 nM	0.9656	389 nM	0.9500

AZA: acetazolamide, hCA I and II: human carbonic anhydrase isoenzymes I and II.
*AZA is used as a standard inhibitor for hCA I and hCA II isoenzymes.

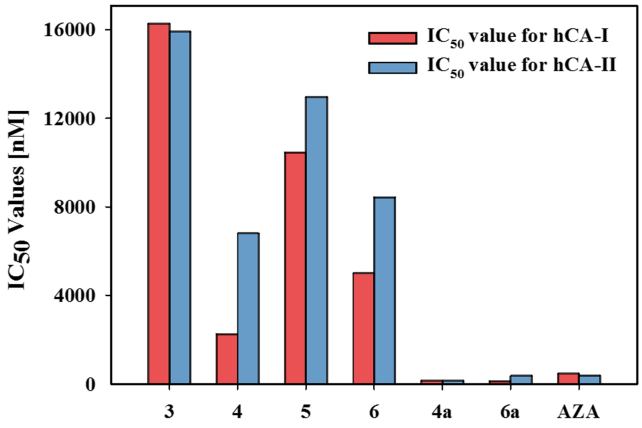

FIGURE 9 Comparison plot of IC_{50} values of **3**, **4**, **5**, **6**, **4a**, and **6a** molecules for hCA I and hCA II

In conclusion, the resulting phthalocyanine complexes **4a** and **6a**, while having moderate α-glucosidase inhibitory activities against acarbose, have higher inhibitory activity on hCA I and hCA II against AZA. However, starting compounds (**3**, **4**, **5**, and **6**), especially **4** and **6**, were found to have the highest IC_{50} than phthalocyanine complexes (**4a** and **6a**) when tested on hCA I and hCA II isoforms against AZA. Besides, the phthalonitrile compounds **4** and **6** were found to have the highest IC_{50} than phthalocyanine complexes (**4a** and **6a**) when tested on α-glucosidase against acarbose and on hCA I and hCA II isoforms against AZA. According to the above results, the different biological activities of the studied molecules against α-glucosidase and carbonic anhydrase isoenzymes compared to their references are due to the substrate–enzyme structure relationship. Because, unlike ligands, when metals enter the core of complexes, the metal chelating effect changes the electron density, facilitating or complicating the inhibitory activity. Thus, with the results we have obtained, important contributions can be made to the literature for new inhibitor's design, synthesis, and development.

3.8 | Molecular docking analysis

Docking studies were performed to investigate the inhibition potential of newly synthesized metallophthalocyanine complexes and their free ligands against hCA I and hCA II. It was also used to define the interactions between the studied compounds with the amino acid residues of the target proteins. Compounds **4**, **4a**, **6**, **6a**, and AZA were individually docked into the determined target

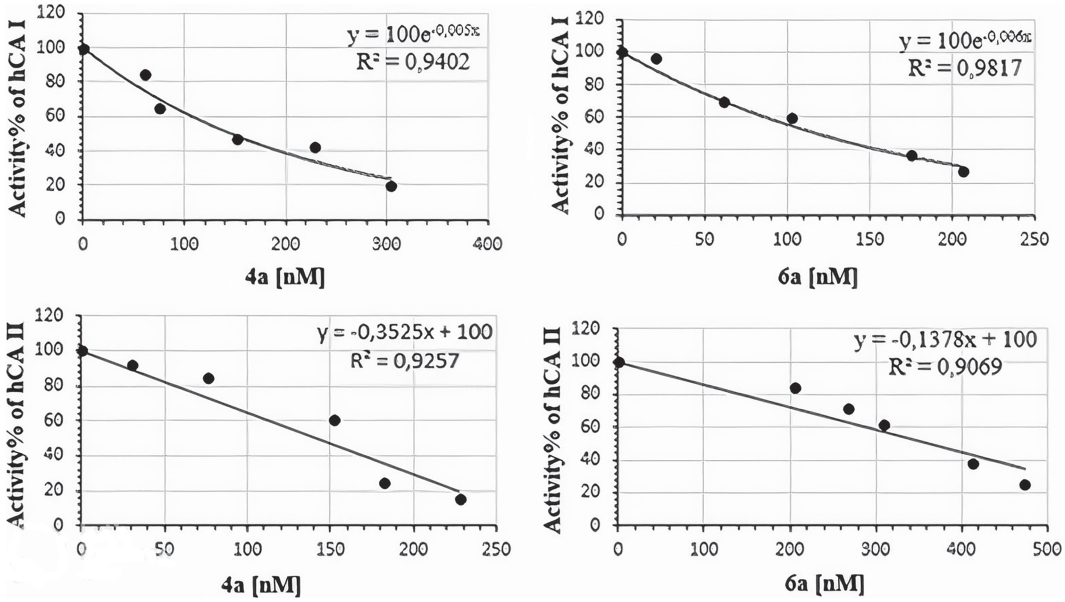

FIGURE 10 IC_{50} graphs of **4a** and **6a** molecules for hCA I and hCA II

TABLE 6 Molecular docking Vina scores (kcal/mol) for compounds **4** and **6** and their zinc–phthalocyanine complexes **4a** and **6a**

	hCA I		hCA II	
PDB ID	**5GMM**	**2FW4**	**3M98**	**5AML**
4	9.1	8.0	8.9	8.9
4a	12.2	12.7	11.9	14.1
6	7.8	8.1	8.0	8.5
6a	9.2	8.6	11.9	10.2
AZA	8.5	8.1	8.6	8.7

proteins as 5GMM, 2FW4, 3M98, and 5AML. The estimated best Vina scores were given in Table 6. Due to the most important factor affecting the enzyme inhibition potential of molecules that occur between ligand and enzymes, the enzyme–ligand interactions were investigated in detail (Figures 11 and 12).

Based on the docking study, it was found that the metal complexes (**4a** and **6a**) were interacting with enzymes more strongly than the reference drug molecules (AZA) and metal-free ligands (**4** and **6**) with a range of Vina score −8.6 and −14.1 kcal/mol due to contact of Pc complexes (**3**–**5**) were very large.

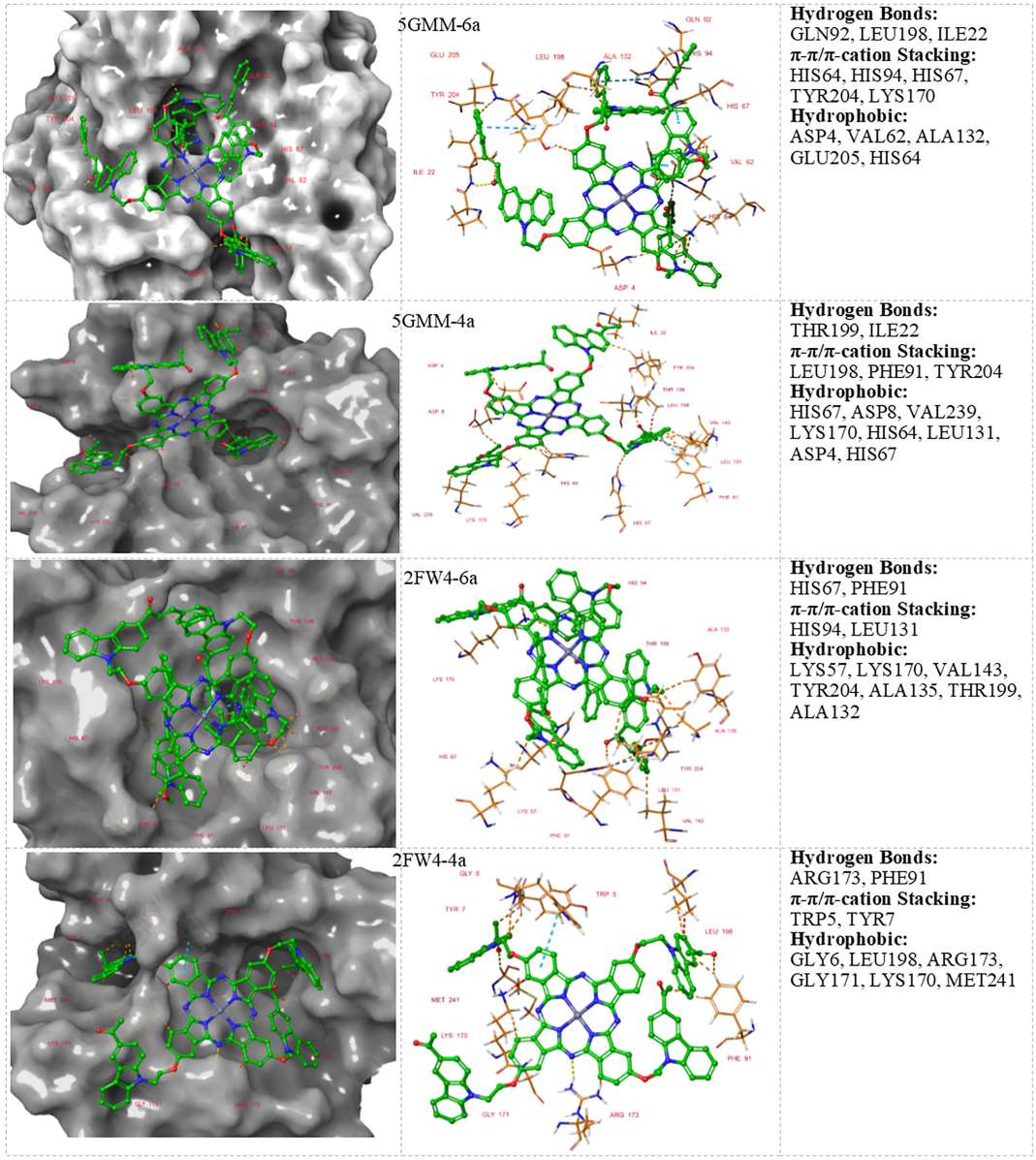

FIGURE 11 The docking pose and interactions of the Pc complexes (**4a** and **6a**) on the binding region of hCA I. Yellow dashed line: H-bond, light-blue dashed line: π–π stacking, green dashed line: π-cation, orange dashed line: polar interactions

The active sites of hCA isozymes were defined as the catalytic Zn^{2+} ion located at the bottom of a cone-shaped cavity surrounded by THR199, LEU198, HIS64, and HIS200. Pc complexes block the entrance to the active site, like an octopus with one or both arms extending toward the active site, whereas free ligands are located only by extending toward the active site. Therefore, although free ligands interact only with the canonical catalytic site where the Zn^{2+} ion is at the bottom, the Pc complexes also interact with other amino acid residues at the entrance of the active site and form a stronger binding with the enzyme. The presence of one ethylene linkage at the junction of the phthalocyanine core and the peripheral groups facilitates the peripheral arms to easily rotate and extend toward the active site. The binding interactions and surface poses of Pc complexes were demonstrated in Figures 11 and 12.

For a more detailed investigation of the interactions of hCA I and Pc complexes, it is seen that one peripheral arm of the Pc complexes extends toward the active site of

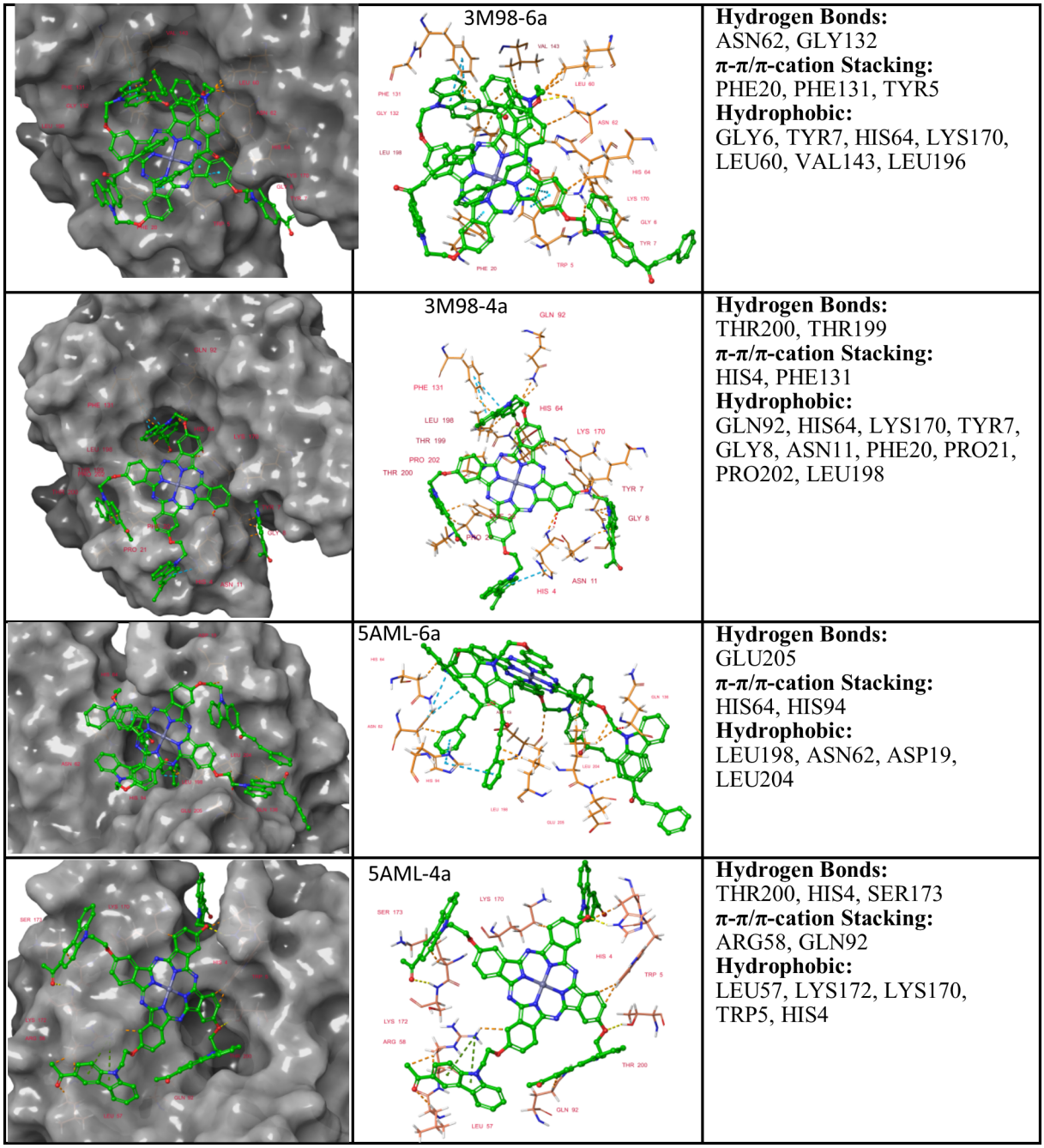

FIGURE 12 The docking pose and interactions of the Pc complexes (**4a** and **6a**) on the binding region of hCA II. Yellow dashed line: H-bond, light-blue dashed line: π–π stacking, green dashed line: π-cation, orange dashed line: polar interactions

both target structures and interacts with the amino acids responsible for the activity there. The compound **6a** forms hydrogen bonding interactions with LEU198, ILE22, and GLN92 amino acids residues; π–π interactions with HIS64, HIS94, HIS67, TYR204, and LYS170 amino acids; and hydrophobic interactions with ASP4, VAL62, ALA132, GLU205, and HIS64 with amino acids at the active site of the 5GMM enzyme structure.

In the interaction of the **4a** molecule with the same enzyme structure, it was seen that they formed hydrogen bonds with the THR199 and ILE22 amino acids and π–π interactions with the LEU198, PHE91, and TYR204 amino acids. Among these interactions, the ones with the LEU198, THR199, and HIS 64 amino acids, which are located around the Zn^{2+} ion in the catalytic region, are even more important in terms of inhibition potential. The interactions of **4a** and **6a** molecules in the 2FW4 enzyme structure are similar to the 5GMM enzyme structure. Both Pc molecules interact with HIS67, PHE91, and ARG173 amino acid residues by making hydrogen bonding. It was also found that TRP5, TYR7, HIS94, and LEU131 amino acid residues form π–π interactions. It is seen that the three peripheral groups of the **4a** molecule approach the catalytic region from different directions by curling over the ethylene linkage attached to the oxygen atom in the junction region to the Pc core skeleton.

When the interaction of hCA II and Zn–phthalocyanine complexes was examined, similar interactions were observed with hCA I at the binding site of the enzyme. Although the **6a** molecule is located as a cap on the cone-shaped active sites of the 3M98 and 5AML enzyme structures, one of the peripheral groups of Pc is directed toward the active site, causing the metallic catalytic site to be inactivated. Due to the shorter peripheral group of the **4a** molecule, the Pc main skeleton adhered more to the enzyme surface, again extending one of the peripheral groups toward the active site. **6a** makes hydrogen bonding interactions with the enzyme through ASN62, GLY132, and GLU205 amino acid residues. π–π stacking and π–cation interactions occur via TRP5, PHE131, PHE20, HIS64, and HIS94 amino acid residues. The hydrophobic interactions contribute to the binding energy through some amino acid residues, such as LEU198, ASN62, HIS64, and LYS170. Hydrogen bonding interactions occur between **4a** and THR200, THR199, THR200, HIS4, and SER173 amino acid residues of hCA-II enzyme, which are close to catalytic Zn ion. The π–π interactions were also observed with HIS4, PHE131, ARG58, GLN92 and GLN92, HIS64, and LYS170 amino acid residues. The hydrophobic interactions between **4a** and TYR7, GLY8, ASN11, PHE20, PRO21, PRO202, and LEU198 amino acid residues also contributed to the binding pattern.

4 | CONCLUSION

In the present work, 4-(2-(3-acetyl-9H-carbazol-9-yl)ethoxy)phthalonitrile (**4**) and 4-(2-(3-cinnamoyl-9H-carbazol-9-yl)ethoxy)phthalonitrile (**6**) were synthesized using 1-(9-[2-hydroxyethyl]-9H-carbazol-3-yl)ethan-1-one (**3**) and (E)-1-(9-[2-hydroxyethyl]-9H-carbazol-3-yl)-3-phenylprop-2-en-1-one (**5**), which were obtained as a result of a series of reactions. By reacting these compounds (**4** and **6**) in the presence of Zn metal salt, **4a** and **6a** new carbazole-substituted Zn (II) Pcs were prepared, and their structures were elucidated using spectroscopic methods, such as elemental analysis, UV–Vis, MALDI-TOF, and FT-IR. Then, to determine the photophysical and photochemical parameters of Pcs (**4a** and **6a**), the aggregation behavior in organic solvents, such as THF, DCM, DMSO, and DMF, was examined, and DMF was chosen as the most suitable solvent with the highest absorbance. When the singlet oxygen yields of synthesized ZnPcs (**4a** and **6a**) were examined, it was thought that the **4a** complex ($\Phi_\Delta = 0.41$) had sufficient singlet oxygen production for PDT applications. The Φ_Δ value of the **6a** complex was lower than that of the **4a** complex due to the large atomic number of **6a**, and therefore, the occurrence of more inter-system transitions. The photodegradation quantum efficiencies for both complexes were studied and showed consistent photostability by not degrading under light irradiation. In addition, these Pcs were effectively quenched by the addition of 1,4-benzoquinone.

The in vitro inhibition activities of all complexes and ligands were examined against α-glucosidase. Compared to standard acarbose, although compounds **5** and **4a** showed more activity, compounds **4** and **6** exhibited the most activity. However, the in vitro inhibitory activity of all complexes and ligands was tested on hCA I and II isoforms. It was found that all complexes and ligands had a strong inhibitory activity on hCA I and hCA II at nM (**4a** and **6a**) concentrations compared to standard AZA. Moreover, these molecules and results were supported by enzyme kinetic and molecular docking studies. In the molecular docking simulations of the newly synthesized Pc complexes, the active site of hCA I and II isoforms attributed the promising inhibitory activity to the key amino acid residues, such as HIS94, LEU198, THR199, and HIS200. Therefore, these inhibition results contribute significantly to the design studies of new, effective, and specific α-glucosidase and CA inhibitors.

ACKNOWLEDGEMENT

We are grateful to TUBITAK (Scientific and Technological Research Council of Turkey, project no.: KBAG-217Z043 and KBAG-115Z446), Sakarya University

for the financial support of these research projects (SAU-BAP, project no.: 2022-7-25-3), and to Sinop University Research Center for the use of the Bruker D8 QUEST diffractometer. S. ÇOL thanks TUBITAK for the doctoral fellowship (BIDEB/2211-C).

AUTHOR CONTRIBUTIONS

Sümeyye Çol: Data curation; formal analysis; resources; investigation. **Mustafa Emirik:** Software. **Zuhal Alım:** Formal analysis. **Arif Baran:** Conceptualization; data curation; formal analysis; funding acquisition; investigation; methodology; project administration; resources; software; supervision; validation; visualization.

CONFLICT OF INTEREST

The authors confirm that this article content has no conflict of interest.

DATA AVAILABILITY STATEMENT

The data that supports the findings of this study are available in the supporting information of this article.

ORCID

Sümeyye Çol https://orcid.org/0000-0003-2932-9718
Mustafa Emirik https://orcid.org/0000-0001-9489-9093
Zuhal Alım https://orcid.org/0000-0001-7216-1194
Arif Baran https://orcid.org/0000-0002-4117-5099

REFERENCES

[1] P. Gregory, Plenum Press, New York, **1991**, *5*(15), 7–273.
[2] N. B. McKeown, Cambridge University Press, New York, **1998**, 32–149.
[3] M. Piskin, Ö. F. Öztürk, Z. Odabaş, *Polyhedron* **2020**, *182*, 114480.
[4] Z. Bıyıklıoglu, T. Arslan, F. A. Alawainati, H. Manaa, A. Jaffar, F. Z. Henari, *Inorg. Chim. Acta* **2019**, *486*, 345.
[5] A. Suzuki, H. Okumura, Y. Yamasaki, T. Oku, *Appl. Sur. Sci.* **2019**, *488*, 586.
[6] G. Guillaud, J. Simon, J. P. Germain, *Coord. Chem. Rev.* **1998**, *178*, 1433.
[7] Y. B. Platonova, A. N. Volov, L. G. Tomilova, *J. Catal.* **2019**, *373*, 222.
[8] S. I. Kawano, Y. Yamada, S. Rongfang, Y. Ishihara, K. Tanaka, *Chem. Lett.* **2018**, *47*, 1262.
[9] X. J. Jiang, S. J. Yeung, P. C. Lo, W. P. Fong, D. K. Ng, *J. Med. Chem.* **2011**, *54*(1), 320.
[10] I. Mohammed, D. O. Oluwole, M. Nemakal, L. K. Sannegowda, T. Nyokong, *Dyes Pigm.* **2019**, *170*, 107592.
[11] V. Almeida-Marrero, E. van de Winckel, E. Anaya- Plaza, T. Torres, A. de la Escosura, *Chem. Soc. Rev.* **2018**, *47*(19), 7369.
[12] M. Li, R. Tian, J. Fan, J. Du, S. Long, X. Peng, *Dyes Pigm.* **2017**, *147*, 99.
[13] S. Vagin, M. Hanack, *Eur. J. Org. Chem.* **2003**, *14*, 2661.
[14] M. V. Martinez-Diaz, G. de la Torre, T. Torres, *Chem. Commun.* **2010**, *46*(38), 7090.
[15] S. Makhseed, M. Machacek, W. Alfadly, A. Tuhl, M. Vinodh, T. Simunek, V. Novakova, P. Kubat, E. Rudolf, P. Zimcik, *Chem. Commun.* **2013**, *49*, 11149.
[16] L. P. Roguin, N. Chiarante, M. C. Garcia Vior, J. Marino, *Int. J. Biochem. Cell Biol.* **2019**, *114*, 105575.
[17] K. J. Kilpin, P. J. Dyson, *Chem. Sci.* **2013**, *4*(4), 1410.
[18] X. H. Peng, S. F. Chen, B. Y. Zheng, B. D. Zheng, Q. F. Zheng, X. Li, M. Ke, J. D. Huang, *Tetrahedron* **2017**, *73*(4), 378.
[19] Y. I. Openda, P. Sen, M. Managa, T. Nyokong, *Photodiagnosis Photodyn. Ther.* **2020**, *29*, 101607.
[20] B. Barut, T. Keleş, Z. Biyiklioglu, C. Ö. Yalçın, *Appl. Organomet. Chem.* **2021**, *35*(1), e6021.
[21] M. Göksel, I. F. Sengul, H. Kandemir, M. Durmuş, *J. Porphyrins Phthalocyanines* **2016**, *20*(06), 708.
[22] E. E. Romero Ale, A. I. Olives, M. A. Martín, B. del Castillo, P. López Alvarado, J. C. Menéndez, *Luminescence* **2005**, *20*(3), 162.
[23] H. Li, Y. Zhang, Y. Hu, D. Ma, L. Wang, X. Jing, F. Wang, *Macromol. Chem. Phys.* **2004**, *205*(2), 247.
[24] M. Bashir, A. Bano, A. S. Ijaz, B. A. Chaudhary, *Molecules* **2015**, *20*(8), 13496.
[25] F. F. Zhang, L. L. Gan, C. H. Zhou, *Bioorg. Med. Chem. Lett.* **2010**, *20*(6), 1881.
[26] Z. A. Kaplancikli, *Marmara Pharm. J.* **2011**, *15*(3), 105.
[27] S. Iqbal, M. A. Khan, K. Javaid, R. Sadiq, S. Fazal-ur-Rehman, M. I. Choudhary, F. Z. Basha, *Bioorg. Chem.* **2017**, *74*, 72.
[28] Y. Camadan, B. Çiçek, Ş. Adem, Ü. Çalişir, E. Akkemik, *J. Biomol. Struct. Dyn.* **2021**, 1.
[29] A. Rifati-Nixha, M. Arslan, N. Gençer, K. Çıkrıkıçı, B. Gökçe, O. Arslan, *J. Biochem. Mol. Toxicol.* **2019**, *33*(6), e22306.
[30] a) W. Benalla, S. Bellahcen, M. Bnouham, *Curr. Diabetes Rev.* **2010**, *6*(4), 247. b) S. S. Nair, V. Kavrekar, A. Mishra, *Eur. J. Experimental Biol.* **2013**, *3*(1), 128. c) M. Taha, M. S. Baharudin, N. H. Ismail, M. Selvaraj, U. Salar, K. A. Alkadi, K. M. Khan, *Bioorg. Chem.* **2017**, *71*, 86.
[31] E. Gallienne, T. Gefflaut, M. Lemaire, *J. Org. Chem.* **2006**, *71*(3), 894.
[32] A. G. H. Bischoff Bayer, *Eur. J. Clin. Invest.* **1994**, *24*(S3), 3.
[33] H. W. Ryu, J. K. Cho, M. J. Curtis-Long, H. J. Yuk, Y. S. Kim, S. Jung, Y. S. Kim, B. W. Lee, K. H. Park, *Phytochemistry* **2011**, *72*(17), 2148.
[34] a) R. Pascale, A. Carocci, A. Catalano, G. Lentini, A. Spagnoletta, M. M. Cavalluzzi, F. De Santis, A. De Palma, V. Scalera, C. Franchini, *Bioorg. Med. Chem.* **2010**, *18*(16), 5903. b) S. Hashmi, S. Khan, Z. Shafiq, P. Taslimi, M. Ishaq, N. Sadeghian, İ. Gulçin, *Bioorg. Chem.* **2021**, *107*, 104554.
[35] S. Kumar, S. Rulhania, S. Jaswal, V. Monga, *Eur. J. Med. Chem.* **2021**, *209*, 112923.
[36] S. Parkkila, K. Kaunisto, L. Rajaniemi, T. Kumpulainen, K. Jokinen, H. Rajaniemi, *J. Histochem. Cytochem.* **1990**, *38*, 941.
[37] M. Aggarwal, C. D. Boone, B. Kondeti, R. McKenna, *J. Enzyme Inhib. Med. Chem.* **2013**, *28*, 267.
[38] D. Sterling, R. A. Reithmeier, J. R. Casey, *J. Biol. Chem.* **2001**, *276*, 47886.
[39] A. A. Farah, W. J. Pietro, *J. Polym. Sci., Part a: Polym. Chem.* **2005**, *43*(23), 6057.
[40] G. Aydin, K. Ally, F. Aktaş, E. Şahin, A. Baran, M. Balci, *Eur. J. Org. Chem.* **2014**, *31*, 6903.

[41] Y. Tao, Y. Zhang, Y. Cheng, Y. Wang, *Biomed. Chromatogr.* **2013**, *27*(2), 148.
[42] F. Saleem, K. M. Khan, S. Chigurupati, M. Solangi, A. R. Nemala, M. Mushtaq, S. Perveen, *Bioorg. Chem.* **2021**, *106*, 104489.
[43] U. K. Laemmli, *Nature* **1970**, *227*(5259), 680.
[44] M. M. Bradford, *Anal. Biochem.* **1976**, *72*(1–2), 248.
[45] J. A. Verpoorte, S. Mehta, J. T. Edsall, *J. Biol. Chem.* **1967**, *242*(18), 4221.
[46] E. Karakilic, Z. Alim, M. Emirik, A. Baran, *Appl. Organomet. Chem.* **2021**, e6537.
[47] H. T. Kim, H. Cha, K. Y. Hwang, *Biochem. Biophys. Res. Commun.* **2016**, *478*(1), 1.
[48] C. Temperini, A. Scozzafava, C. T. Supuran, *Bioorg. Med. Chem. Lett.* **2006**, *16*(19), 5152.
[49] E. Čapkauskaitė, L. Baranauskienė, D. Golovenko, *Bioorg. Med. Chem.* **2010**, *1*(21), 7357.
[50] J. Ivanova, J. Leitans, M. Tanc, A. Kazaks, R. Zalubovskis, C. T. Supuran, K. Tars, *Chem. Commun.* **2015**, *51*(33), 7108.
[51] Schrödinger Release 2018-4: Protein Preparation Wizard. Epik, Schrödinger, LLC, New York, NY, 2016; Prime, Schrödinger, LLC, New York, NY, **2018**.
[52] M. J. Frisch, G. W. Trucks, H. B. Schlegel, M. J. Frisch, G. W. Trucks, H. B. Schlegel, G. E. Scuseria, M. A. Robb, J. R. Cheeseman, G. Scalmani, V. Barone, B. Mennucci, G. A. Petersson, Gaussian 09, revision A.02, **2009**.
[53] J. Tomasi, B. Mennucci, R. Cammi, *Chem. Rev.* **2005**, *105*(8), 2999.
[54] G. M. Morris, D. S. Goodsell, R. S. Halliday, *J. Comput. Chem.* **1998**, *19*(14), 1639.
[55] Y. Liu, M. Grimm, W. T. Dai, M. C. Hou, Z. X. Xiao, Y. Cao, *Acta Pharmacol. Sin.* **2020**, *41*(1), 138.
[56] M. S. Ağırtaş, B. Cabir, S. Özdemir, *Dyes Pigm.* **2013**, *96*(1), 152.
[57] J. Jiang (Ed.), Springer, Berlin Heidelberg, **2010**, *35*, 45–87.
[58] N. M. O'Boyle, A. L. Tenderholt, K. M. Langner, *J. Comput. Chem.* **2008**, *29*(5), 839.
[59] H. Enkelkamp, R. J. Nolte, *J. Porphyrins Phthalocyanines* **2000**, *4*(5), 454.
[60] D. D. Dominguez, A. W. Snow, J. S. Shirk, R. G. S. Pong, *J. Porphyrins Phthalocyanines* **2001**, *5*(7), 582.
[61] M. Çamur, M. Durmuş, M. Bulut, *Polyhedron* **2012**, *41*(1), 92.
[62] T. Nyokong, E. Antunes, Eds., K. M. Kadish, K. M. Smith, R. Guilard, World Scientific, Singapore, chapt. **2010**, *34*(7), 247–349.
[63] E. T. Saka, M. Durmuş, H. Kantekin, *J. Organomet. Chem.* **2011**, *696*(4), 913.
[64] Y. Zorlu, F. Dumoulin, M. Durmuş, V. Ahsen, *Tetrahedron* **2010**, *66*(17), 3248.
[65] J. R. Darwent, I. McCubbin, D. Phillips, *J. Chem. Soc. Faraday Trans.* **1982**, *78*, 347.
[66] M. Idowu, T. J. Nyokong, *J. Photochem. Photobiol., a* **2009**, *204*, 63.
[67] A. Baran, S. Çol, E. Karakılıç, F. Özen, *Polyhedron* **2019**, *175*, 114205.
[68] J. Rose, *Advanced Physico-Chemical Experiments*, Pitman, London, UK **1964**.
[69] N. A. Kuznetsova, N. S. Gretsova, E. A. Kalmykova, E. A. Makarova, S. N. Dashkevich, V. M. Negrimovskii, E. A. Luk'Yanets, *Russ. J. Gen. Chem.* **2000**, *70*(1), 133.
[70] W. Spiller, H. Kliesch, D. Wöhrle, S. Hackbarth, B. Roder, G. Schnurpfeil, *J. Porphyr. Phthalocyanines* **1998**, *2*(2), 145.
[71] I. Gürol, M. Durmuş, V. Ahsen, T. Nyokong, *Dalton Trans.* **2007**, *34*, 3782.
[72] P. Khoza, E. Antunes, T. Nyokong, *Polyhedron* **2013**, *61*, 119.
[73] M. Durmuş, T. Nyokong, V. Ahsen (Eds.), Springer Dordrecht Heidelberg, London, New York **2012**, 135–266.
[74] S. Bhattacharya, C. Biswas, S. S. K. Raavi, J. Venkata Suman Krishna, N. Vamsi Krishna, L. Giribabu, V. R. Soma, *J. Phys. Chem. C* **2019**, *123*(17), 11118.
[75] F. Demir, H. Y. Yenilmez, A. Koca, Z. A. Bayır, *J. Electroanal. Chem.* **2019**, *832*, 254.
[76] P. S. S. Wakabayashi, R. da Costa Duarte, L. G. T. A. Duarte, F. da Silveira Santos, R. Cercená, E. Zapp, A. G. Dal-Bó, *Dyes Pigm.* **2020**, *182*, 108668.
[77] R. Olgac, T. Soganci, Y. Baygu, Y. Gök, M. Ak, *Biosens. Bioelectron.* **2017**, *98*(2), 202.
[78] Y. Derin, R. F. Yılmaz, İ. H. Baydilek, V. E. Atalay, A. Özdemir, A. Tutar, *Inorg. Chim. Acta* **2018**, *482*, 130.
[79] a) B. Yılmaz, E. Güzel, N. Menges, İ. Şişman, M. K. Şener, *Solar Energy* **2018**, *174*, 527. b) F. Saleem, K. M. Khan, S. Chigurupati, Y. Andriani, M. Solangi, S. Hameed, S. Perveen, *Arab. J. Chem.* **2022**, *15*(3), 103651. c) S. Wang, X. Weng, L. Zhang, X. Zhou, *J. Porphyr. Phthalocyanines* **2009**, *13*(08n09), 893. d) R. Kaushal, M. Kaur, *J. Coord. Chem.* **2021**, *74*(4–6), 725.
[80] D. Y. Lee, H. W. Kim, H. Yang, S. H. Sung, *Phytochemistry* **2017**, *137*, 109.

SUPPORTING INFORMATION

Additional supporting information can be found online in the Supporting Information section at the end of this article.

How to cite this article: S. Çol, M. Emirik, Z. Alım, A. Baran, *Appl Organomet Chem* **2022**, *36*(9), e6799. https://doi.org/10.1002/aoc.6799